

Impact of Skin Hyper- and Visco-elastic Properties on the Neural Mechanotransduction for
the Slowly Adapting Type I Afferent

A Thesis

Presented to
the faculty of the School of Engineering and Applied Science
University of Virginia

in partial fulfillment
of the requirements for the degree

Master of Science

by

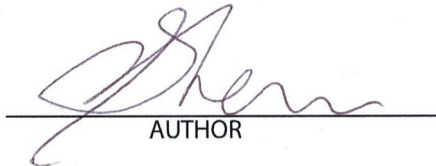
Yuxiang Wang

December

2012

APPROVAL SHEET

The thesis
is submitted in partial fulfillment of the requirements
for the degree of
Master of Science


AUTHOR

The thesis has been read and approved by the examining committee:

Gregory J. Gerling

Advisor

Stephen D. Patek

Richard W. Kent

Accepted for the School of Engineering and Applied Science:



Dean, School of Engineering and Applied Science

December
2012

Contents

Abstract	2
1. Overall Thesis Introduction	3
2. Analysis on Skin Hyperelasticity	6
2.1. Introduction	6
2.2. Results	9
2.2.1. Impact of body weight	12
2.2.2. Impact of hair cycle stages	14
2.2.3. Impact of skin sites	15
2.3. Discussion	16
2.4. Materials and Methods	22
3. Analysis on Skin Viscoelasticity	29
3.1. Introduction	29
3.2. Methods	32
3.3. Results	37
3.4. Discussion	39
4. Impact of Skin Properties on SAI	43
4.1. Introduction	43
4.2. Methods	45
4.2.1. Mouse Skin Measurements	45
4.2.2. Numerical Model	49
4.2.3. Exploratory Numerical Experiments	51
4.3. Results	52
4.4. Discussion	57
5. Overall Thesis Conclusion	59
Appendix A: Derivations of equations for Section 2	61
Derivation of Eqn. (2.5)	61
Derivation of Eqn. (2.6)	61
Derivation of Eqn. (2.7)	61
Appendix B: Case study for Section 3 in strain-dependency on one sample	63
Methods	63
Results	64
Discussion	67
Acknowledgment	68
Reference	69

Abstract

Our sense of touch is of vital importance to activities of daily living, from interacting with one's surroundings to manipulating tools. Therefore, understanding the input-output relationship (or transfer function) of a mechanical stimulus at the skin to the neural response from the afferent is important. Upon contact with mechanical stimuli, tactile mechanoreceptors respond to skin deformation by transducing stresses and strains in tissues local to end organs into trains of action potentials. In addition to the morphology of an end organ and dynamics of a particular neuron, the skin's mechanics may impact neural spike firing patterns. Most prior work in skin modeling has simplified its structure to be linear elastic and not often included time dependent viscoelasticity. Furthermore, the specimen to specimen variation of skin is seldom considered. The effort here focuses upon hyper- and visco-elastic modeling of skin mechanics, and the impact of their variation upon the neural spike firing patterns inherent to its input-output mechanotransduction function.

1. Overall Thesis Introduction

Tactile perception is a function of several sub-steps: the mechanical stimulus in the environment contacts and deforms the skin, these spatial distributions of forces propagate through the skin to the locations of the end organs, the local stresses/strains are transduced into bioelectric trains of action potentials, and these signals are carried by A β - or A δ - afferent nerves to the central nervous system. In mammals, tactile perception is based on four types of cutaneous mechanoreceptor afferents: slowly adapting type I (SAI), slowly adapting type II (SAII), rapidly adapting (RA) and Pacinian corpuscles (PC) [1]. The four types respond uniquely to certain facets of time and spatially dependent stimuli and are found in differing population densities. Work herein is mainly concerned with SAI afferents, which are densely innervated (100 per cm²) and are sensitive to edges, corners and curvatures. The end organ of SAI afferent is Merkel cell-neurite complexes. Moreover, for the SAI afferent, at least four major factors impact its transfer function: a) mechanical properties of the skin that modulate the distal stimulus to stresses/strains local to the Merkel cells; b) transduction properties at individual Merkel cells and their spike initiation zones; c) branch-structured morphology of the Merkel cell neurite complex which integrates information at each individual Merkel cells; d) fiber type that carries the bioelectric signal at a conduction velocity.

The skin properties alone likely impact neural spike firing. We already know for example,

that the location of end organs in epidermal skin may enhance neural response [2][3][4], as we know that the structure of the end organ (i.e., layers of the Pacinian corpuscle) impact its neural response [5].

The skin is known to behave dramatically different between loading in tension and compression. Tensile tests show the skin to be highly non-linear and viscoelastic, which is mainly due to the matrix morphology of collagen fibers [6]. Similarly, indentation to explore its compressive properties have showed non-linearity and viscoelasticity [7], but considered these caused by the viscosity of interstitial fluid. The initial modulus in tension are of similar values (5 kPa, [6]) with that of compression we measured (3.78 kPa); however, the skin is much stiffer (3 MPa) at 20% - 30% strain [8] than that in compression (30 kPa) from our measurement. In addition, during most human activity utilizing active touch sensing, stimuli produce mainly compressive stress/strains instead of tensile.

Furthermore, the skin's mechanical properties change with environmental factors, such as age apart from the morphology of the end organs from test using torque load [9][10]. These data, however, cannot be directly used as input for general skin models, since we need general measurement data from tensile and compressive regime. Since there are no measurement data available, Dandekar et. al developed a 3D model with the material parameters from fitting the finite element model to measured skin deflection [11], and

Phillips and Johnson used an analytical model with linear assumption which did not use Young's modulus value in calculating the output strain value [12].

The gap in the knowledge base is the need to understand how the variation in skin mechanics between animals and body sites under a compressive loading regime. This information is needed for more in-depth modeling of SAI mechanotransduction. Therefore, this is the focus herein.

The work herein aims to address this gap using standard uniaxial compression material tests, finite element models, and statistical tests and models to explore the extent of skin mechanics variation in hyperelasticity, viscoelasticity and their impact upon two different experimental indentation techniques (force versus displacement control).

More specifically, the three aims of this thesis are:

- 1) Measure skin hyperelastic properties in compression regime and find their correlation with factors of body weight, hair cycle stages and skin sites;
- 2) Measure skin viscoelastic properties in compression regime and find their correlation with factors of strain level, loading velocity and skin thickness;
- 3) Compare two electrophysiological neural-recording stimuli techniques (force and displacement control) based on skin measurement and finite element models.

2. Analysis on Skin Hyperelasticity

2.1. Introduction

The skin is a complex structure that consists of unique layers of epidermal, dermal and subcutaneous fat [13] which overlay muscle tissue and bone. Mechanically, the skin is a non-linear, hyperelastic material [7] that exhibits as well time-dependent viscoelastic relaxation and creep tied to the properties of elastin, proteoglycan, collagen and interstitial fluid [14], [15]. As well, embedded collagen bundles give rise [16] to greater forces in tension than compression. The geometry and characteristics of interfaces between individual skin layers are often undulating and tied tightly together, the structure and function of which vary between skin sites [17], as does overall thickness. At present, a better understanding of the skin's mechanical properties is sought by those developing cosmetics, surgical procedures, and studying touch perception, however the measurement of the skin's many dimensions is a complex undertaking.

The skin's mechanics have been measured using uniaxial and biaxial tensile tests, uniaxial compression, torque loading, and indentation [9]. The latter two are indirect methods, which for soft materials tend to generate highly non-linear stress fields, therefore making it difficult to calculate constitutive laws relating material stress to strain. The former two more readily afford constitutive models and importantly material quantification in an absolute, as compared to comparative fashion. Most typically, the

tensile regimes are used. For example, in uniaxial tensile tests with human cadaver tissue, the stress-strain curve was found to be linear under small deformations, non-linear at intermediate strains and again linear at large strain levels [9]. Others have conducted bi-axial tensile tests, both in rats [18] and human cadavers [19]. Comparatively in compression, many fewer tests have been conducted. This is due in part to experimental difficulties and the availability of predefined material models. In one notable case, compression loading was done with pigskin, considering the skin's non-linearity and viscoelasticity, though done on a single specimen basis with small ($< 10\%$) deformation [7].

The skin behaves dramatically different in tension than in compression. While in small deformation the elastin plays a role in either tension or compression, in larger deformation, the collagen fibers pull tight under tension for an increase in force whereas under compression they play little to no role. As a consequence, although the modulus at 5-10% strain in tension (5 kPa, [6]) is similar to that measured in compression (7.34 kPa, [7]), the modulus at 20 - 30% strain in tension is increased by approximately two orders of magnitude (~ 6 MPa, [8]) as compared to that measured in compression (37.97 kPa, [7]).

Furthermore, the skin's mechanical properties change with age, and between both skin sites and skin layers. With increasing age, skin thickness decreases [20], and its tensile non-linear modulus increases [9] and distensibility decreases [21]. In addition, we know

that the thickness of the skin layers depends significantly upon skin sites for both the epidermis [22] and dermis [23] and that a stiffness change may likely accompany. However, there is no existing study on how the hyperelasticity of skin changes with factors of age and weight.

The specific gap in the knowledge base is that there is little existing data on the hyperelasticity of the skin, especially given changes that accompany aging, between skin sites, body weights and animals, and done in a state of compression. There are also not enough samples to begin to capture the distribution of variation beyond the mean.

The work herein addresses this gap by use of compressive uniaxial tests on freshly excised mouse skin across different ages and body weights. In particular, we utilize controlled displacement, linearly ramped into the skin surface, at velocities of 10 μm per second to collect force-displacement data from which we generate hyperelastic material parameters to characterize skin stiffness and modulus. Also calculated was skin thickness, based on a procedure developed herein that contrasts with typical methods that utilize calipers [19]. Measured specimens were comprised of 105 skin samples freshly excised from 24 mice, ranging in age 5.71 – 6.86 weeks, 9.00 – 10.29 weeks, 12.57 – 12.71 weeks, 16.86 – 19.29 weeks, and 34.29 – 26.29 weeks, comparing separable phases of the hair cycle (groups young active – YA, young resting – YR, intermediate active – IA, intermediate resting – IR, and mature – M), and from skin sites at distal, proximal on

nerve trunk and proximal off nerve trunk on hind limb.

In specific, these data were analyzed according to three research questions:

- (1) What are the material properties, namely the thickness, stiffness, and modulus of each specimen?
- (2) Are skin material properties dependent on the animal's body weight, hair cycle stage and sampling skin site?
- (3) What is the relationship between skin material parameters, namely skin thickness, stiffness and modulus in this work?

2.2. Results

Uniaxial compression tests (Figure 2.2a) were performed on 105 circular skin punches of 6 mm diameter sampled from mouse hind limb, where force and displacement were recorded and later translated into stress and strain curves. We varied factors of age (5.7 - 34.3 weeks, Figure 2.1a, b and c), body weight (15.94 to 61.39 grams, Figure 1d), skin site (distal, proximal off nerve trunk, proximal on nerve trunk, Figure 2b), hair cycle stages (5.71 – 6.86 weeks – groups Young Active – YA, 9.00 – 10.29 weeks – Young Resting – YR, 12.57 – 12.71 weeks – Intermediate Active – IA, 16.86 – 19.29 weeks – Intermediate Resting – IR, 26.29 – 34.29 weeks – Mature – M) on the 24 animals being sampled. For convenience of analysis, YA and IA are sometimes grouped together as

Active group, and similarly YR and IR grouped together called Resting group. The thickness of the specimens were obtained from contact force of the probe with the skin surface, while the fit of stress versus strain to modified exponential functions resulted in hyperelastic parameters of stiffness and modulus, as detailed in Methods.

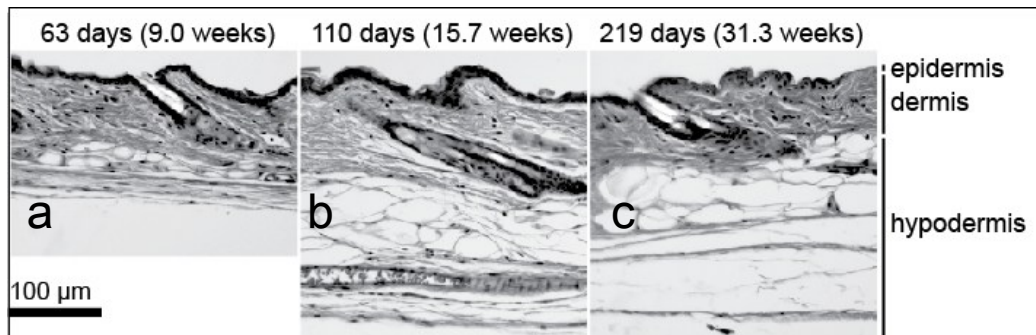


Figure 2.1 a, b and c: Longitudinal cross-section histology pictures taken from sampling sites at 63 days, 110 days and 219 days. d. Body weight vs. age plot. Circles shows the grouping of age groups.

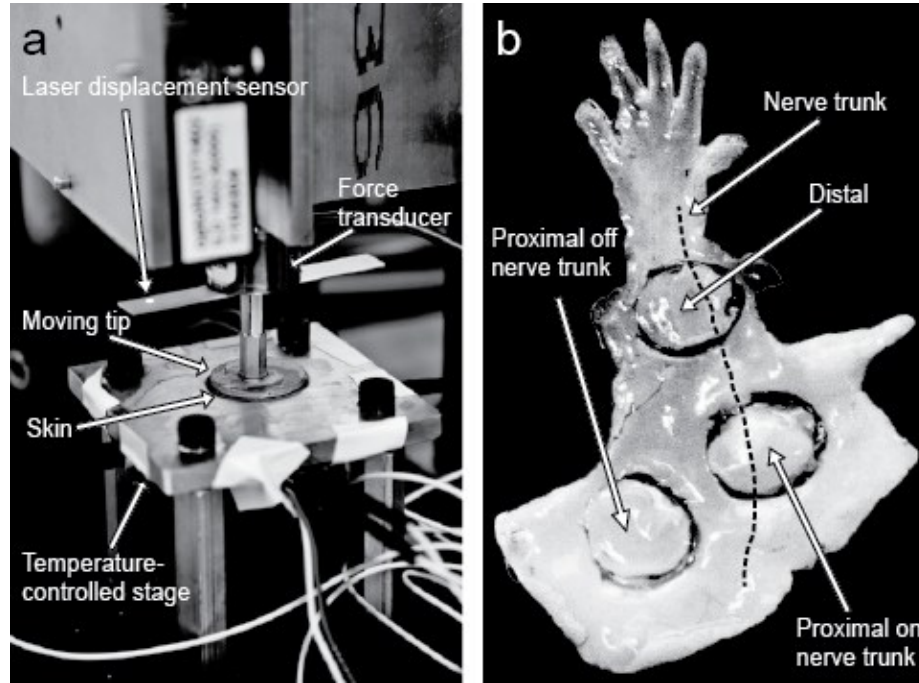


Figure 2. 2 a: Photo of measurement apparatus. b: Hindlimb skin flap of the mouse, taken from a typical 10-week animal, illustrating the sampling locations.

Three independent variables (body weight, hair cycle stages and skin sites) and their impact on three dependent variables (thickness, stiffness coefficient p and modulus coefficient q) will be analyzed.

Generally remarks. All three dependent variables are highly variant: thickness= $278.33 \pm 102.49 \mu\text{m}$ (CV=0.368), stiffness coefficient $p=42.06 \pm 11.79 \text{ mm}^{-1}$ (CV=0.280), and modulus coefficient $q=10.77 \pm 2.03$ (CV=0.188). Less variation for thickness is observed within only active group ($313.55 \pm 75.93 \mu\text{m}$, CV=0.242) or only resting group ($234.52 \pm 55.74 \mu\text{m}$, CV=0.238), and higher variation occur within only mature group ($333.19 \pm 144.98 \mu\text{m}$, CV=0.435).

2.2.1. Impact of body weight

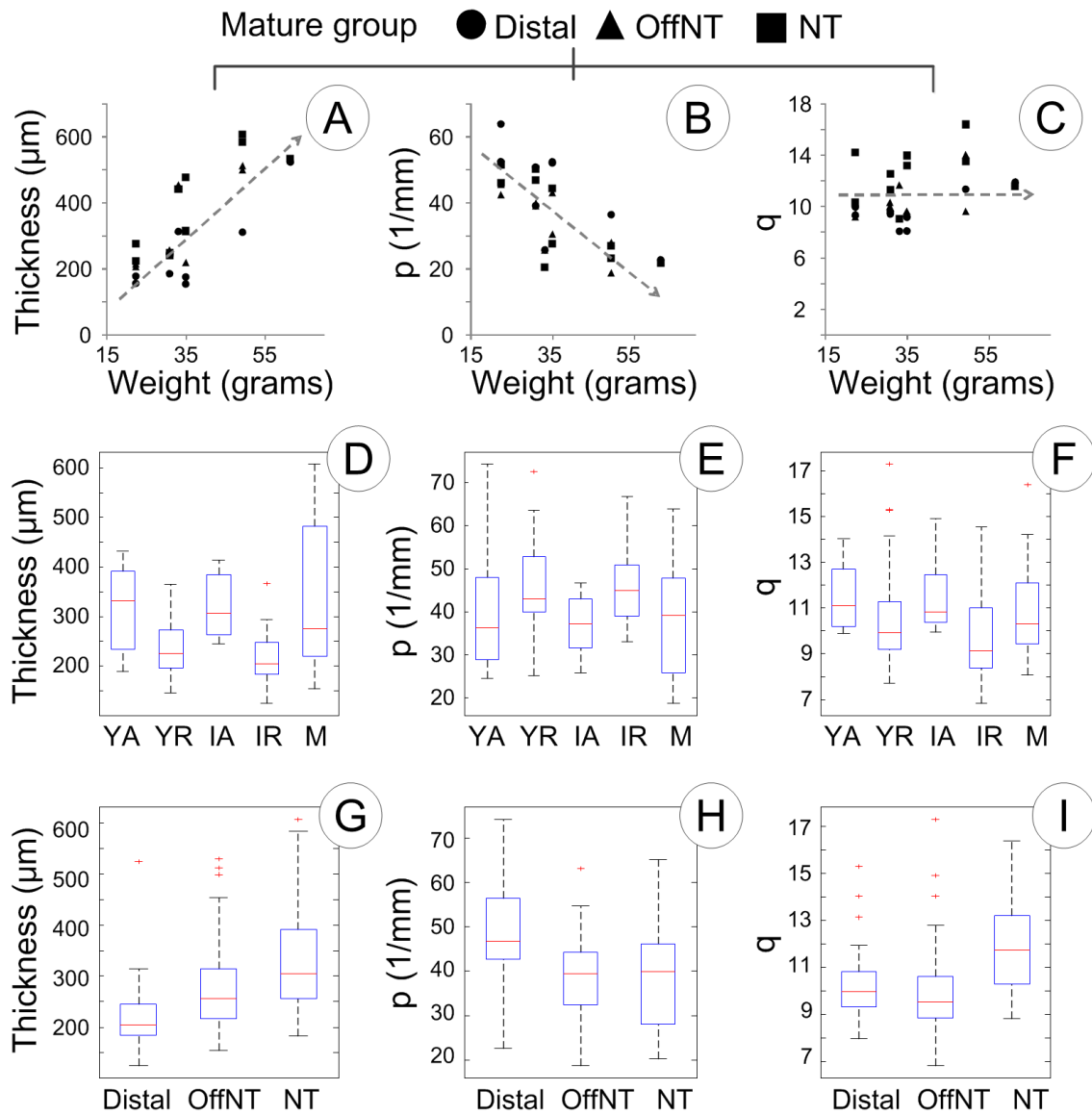


Figure 2.3 Skin thickness, stiffness coefficient p and modulus coefficient q change with respect 1) to animal body weight (A, B and C); 2) to animal hair cycle stages (D, E and F); 3) to sampling skin sites (G, H and I).

On thickness. The body weight of the animal is positively correlated to skin thickness ($r=0.793$, $p\text{-value}<1e-6$) for the mature group animals (Figure 2.3A). No such correlation was found among animals in either active cycling animals or resting animals ($r=0.215$

and -0.127 respectively, p-values>0.3 for both).

On stiffness coefficient p. The body weight of the animal is negatively correlated to the stiffness coefficient p ($r=-0.717$, $p\text{-value}<1e-3$) for the mature group animals (Figure 2.3B). No such correlation was found ($r=-0.272$ and 0.039 respectively, $p\text{-value}>0.2$) among animals in either active cycling animals or resting animals.

On modulus coefficient q. The body weight of the animal is not significantly correlated to the modulus coefficient q ($|r|<0.7$ for all sites) for mature group (Figure 2.3C), active haircycling and resting group. All p-values and coefficient of correlation between skin parameters and animal body weights from the Pearson test of correlation are listed in Table 2.1.

Table 2.1 P-values and correlation coefficients from statistic tests

Body weight			p-value			Correlation coef. r		
			Mature	Active	Resting	Mature	Active	Resting
	Thickness	Distal	0.003	0.124	0.230	0.862	0.589	-0.298
		OffNT	0.001	0.280	0.688	0.870	0.529	-0.102
		NT	0.003	0.719	0.651	0.835	-0.152	-0.114
		All sites	0.000	0.336	0.362	0.793	0.215	-0.127
	p	Distal	0.026	0.267	0.750	-0.727	-0.447	0.081
		OffNT	0.004	0.376	0.226	-0.813	-0.446	-0.301
		NT	0.014	0.657	0.253	-0.744	0.187	0.284
		All sites	0.000	0.220	0.781	-0.717	-0.272	0.039
q	Distal	0.044	0.911	0.354	0.679	-0.047	-0.232	
	OffNT	0.065	0.754	0.155	0.603	-0.165	-0.350	
	NT	0.478	0.981	0.252	0.255	0.010	0.285	

		<i>All sites</i>	<i>0.039</i>	<i>0.786</i>	<i>0.513</i>	<i>0.386</i>		<i>-0.062</i>	<i>-0.091</i>
Hair cycle			YR	IA	IR	M		OffNT	NT
	Thickness	YA	0.001	0.747	0.007	0.581	Distal	0.007	0.000
		YR		0.000	0.249	0.000			
		IA			0.002	0.795	OffNT		0.022
		IR				0.012			
	p	YA	0.154	0.563	0.199	0.557	Distal	0.000	0.000
		YR		0.031	0.704	0.006			
		IA			0.030	0.928	OffNT		0.790
		IR				0.033			
	q	YA	0.138	0.824	0.030	0.449	Distal	0.879	0.000
		YR		0.155	0.310	0.363			
		IA			0.051	0.414	OffNT		0.001
		IR				0.109			

P-values<0.05, or |r|>0.7 are highlighted.

2.2.2. Impact of hair cycle stages

On thickness. The hair cycle stages of the animal is having a significant impact on skin thickness (Figure 2.3D), as the trend shows a W-shape trend with the growth of an animal. Student's t-tests were performed to compare the between-group difference (Table 2.1), and it showed that all the thicknesses from active groups (YA and IA) are not distinguishable from each other, as well as resting groups (YR and IR), but there is a significant difference between each of the active groups to resting groups.

On stiffness coefficient p. The hair cycle stages of the animal is also having a significant impact on stiffness coefficient p (Figure 2.3E), and with an M-shape trend with the growth of an animal (which is similar but the opposite compared to the trend in thickness

change). Student's t-tests were also performed, and p-values were listed in Table 2.1.

On modulus coefficient q. The hair cycle stages of the animal is not having significant impact on modulus coefficient q (Figure 2.3F), as student's t-test does not show significance among most between-group comparisons (Table 2.1).

2.2.3. Impact of skin sites

On thickness. The skin sites of the specimen sampled is having a significant impact on skin thickness (Figure 2.3G), as the specimens sampled from distal site being thinnest, OffNT thicker and NT the thickest. Student's t-tests showed this as a significant trend (Table 2.1).

On stiffness coefficient p. The skin sites of the specimen sampled is also having a significant impact on stiffness coefficient p (Figure 2.3H), as stiffness from distal site higher than the others (p-value<1e-3, Table 2.1).

On modulus coefficient q. The skin sites of the specimen sampled is having significant impact on modulus coefficient q (Figure 2.3I), as stiffness from NT site higher than others (p-value<1e-3, Table 2.1).

2.3. Discussion

Relationship Between Thickness, Stiffness and Modulus

It is interesting to note that both change in body weight and hair cycle stages will introduce change in both thickness and stiffness in opposite directions, resulting in a relatively consistent modulus coefficient q (according to Eqn. (2.7), q is the product of thickness and p). The observation that the amount of change in thickness approximately counteracts the amount of change in stiffness coefficient indicates that all skin samples have consistent modulus given skin site (Figure 2.4A, B and C). Overall regression was also performed (Figure 2.4D), returning the slope (value of q) is 10.745, with $R^2=0.739$.

This may explain that the modulus of the skin remains relatively unchanged when the animal is growing, i.e. the mechanical properties of skin are independent of its thickness, age and animal body weight. Daly reported an increasing trend between age and moduli [9], however his test demonstrated this conclusion only in the tensile condition and therefore there is no conflict between his work and work presented here. In addition, the correlation between skin thickness and body weight has been seldom looked into; except for Krueger et. al [21], the differences of skin mechanics across skin sites has not been studied.

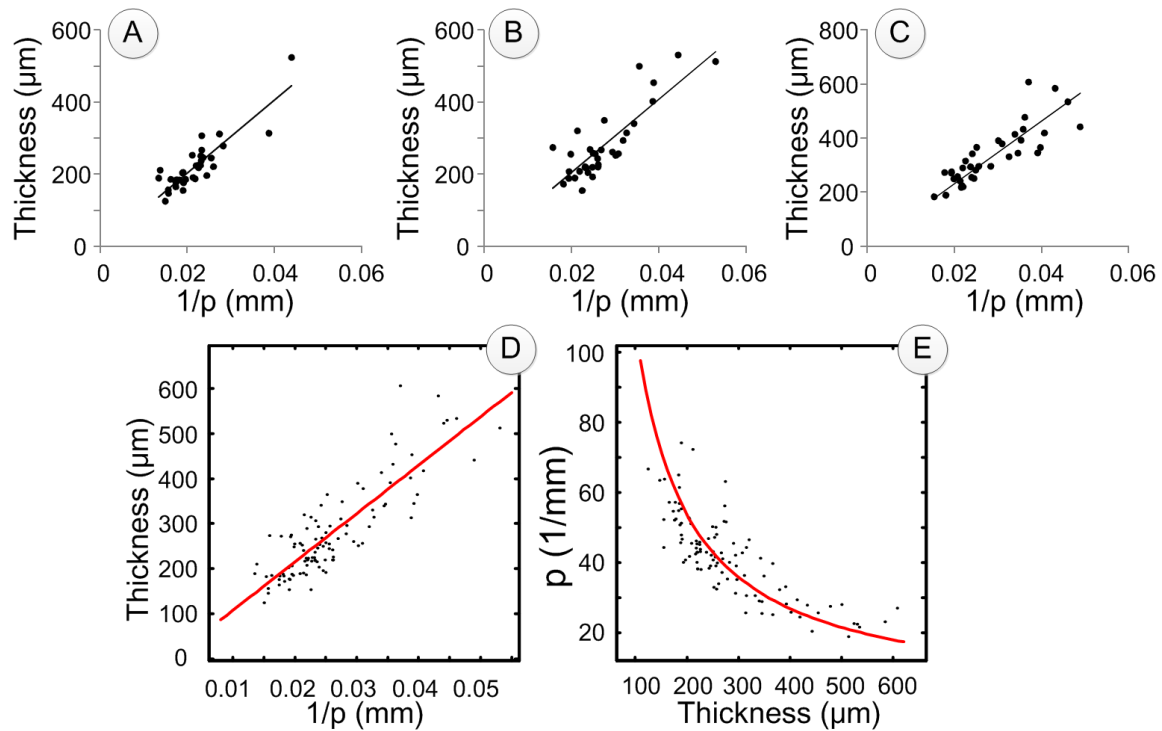


Figure 2.4 A, B and C: Plots with $1/p$ on the X axis and thickness on the Y axis. Solid lines are linear regression curves, average $R^2=0.723$. The slope of the regression lines are the modulus coefficient q . D: Linear regression (line) for all skin samples (dots) between $1/k$ and thickness returns $\text{thickness}=10.745/p$, $R^2 = 0.74$. E: Observed reciprocal relationship, demonstrating p is a function of thickness.

Overall Biological Conclusions

Overall, the skin thickness, stiffness, and modulus all vary between different groups varying ages, body weights, skin sites, hair cycle stages and maturity. Three major conclusions emerge from analysis: 1) in mature animals, the body weight is prominently correlated with skin thickness (positive) and with skin stiffness (negative), resulting in a consistent modulus; 2) hair cycle stages dominate skin thicknesses and stiffness in younger animals, while skin is significantly thicker and less stiff in active hair-cycling

animals, but also resulted in a consistent modulus coefficient (not significantly variant according to statistical tests); 3) skin sites being sampled also have an impact on skin properties, while distal skin being thinnest and stiffest, NT skin being thickest and highest modulus.

Overall variability. Generally, the high variability of skin thickness and stiffness shows that the mechanics of the skin are largely dependent on individual specimens. There are some dependent variables with skin mechanics being traced, namely body weight, hair cycle stages and skin site. Still there may be other factors leading to the variability. For example, making sure the three punches per animal came from the exact same anatomical locations is very hard to control. To some small extent as well, accounting for differences in animal age down to the resolution of a day may also play a role. Note also that the GFP mice utilized are controlled by diet and habitual environment, which excluded other confounding factors to this variance. One would expect even higher variance in human subjects.

Impact of body weight. We observed that skin thickness was correlated positively, stiffness coefficient negatively with body weight in mature animals, and changes in thickness and stiffness resulted in a consistent modulus value. Animals with heavier weight have more hypodermal fat compared to lighter animals, and therefore a thicker hypodermal layer. Therefore, skin from the younger animals with less amount of fat

(active and resting groups) does not show significant correlation with body weight and skin thickness.

Impact of hair cycle stages. We observed that skin thickness and stiffness are both impacted by the haircycle stages of the animal, though in different directions. Skin thickness in active-cycling groups are significantly thicker than those in resting groups, therefore changing with a W-shaped pattern in mouse's life cycle. Similar trend goes to stiffness coefficient, but in the opposite direction i.e. follows an M-shaped pattern. These two opposite trends counteracted each other and resulted in a consistent modulus value. This can be decomposed into two factors: increase in age causing the change of hair cycle status, and increase in age in the same state of hair cycling. The results herein indicate that only the hair cycle effect of aging is impacting skin, while different ages in same hair cycle stages (i.e. YA and IA, YR and IR) does not make a difference in skin. As we compare our results to existing literature, we see that the impact of aging on skin properties is complicated. As measured in human subjects [20], the thickness of skin peaks at about 25 years old, increasing with age before that point and decreasing thereafter. Considering hair cycling does not appear in human, results from our measurements does not contradict with reported result in human. The correlation of age and thickness disappeared in the mature group, due to a large variation of body weight which buried the trend caused by age alone.

Impact of skin sites. We observed that the skin thicknesses, stiffness are both changing with the change of sampling skin site. Moreover, unlike the factors of body weight and hair cycle stages, these changes do not counteract each other. The modulus in the NT site is higher than the other two. This can explain that during the growth of an animal, its skin at the same site may remain the same modulus along the life span, but different skins at different sites can have different moduli.

Note on the dependency of skin site, maturity level and the independency of hair cycle stages with skin thickness. As we vary either skin site, maturity level or hair cycle stages, we change the structural compositions of the skin specimen. For skin site, proximal skins tend to have a thicker layer of hypodermal fat compared to skins sampled from distal area, and skin on nerve trunk contains an extra volume of nerve trunk compared to skin off nerve trunk. For maturity level, animals are less synchronized in their state of growth as they age and have a much greater variation of their body weight. Therefore, the variation of skin thickness are much larger compared to animals in the younger group. For hair cycles, taking active stage as an example, there are significantly larger hair follicles in size embedded in the skin [24], which has now been shown not having an effect on skin thickness.

Novel Methods Used in this Study

The material properties of skin were quantified, for the first time, i) under compression, ii) for freshly excised tissue, iii) for a population of specimens, and iv) where age, weight, maturity level, hair cycle stages and skin site were systematically varied. In this study, a total number of 105 freshly excised skin specimens from 24 animals, from 3 skin sites, 5 hair cycle stages and 3 skin sites were studied; animal age ranges from 40 to 240 days, body weight from 15.94 grams to 61.39 grams. In comparison, others have studied how age-related skin mechanical properties change under other conditions such as tensile loading [9], torsional loading [20] and by using a cutometer [21]. Studies of the skin under compression are highly limited in the literature except for one with pig cadaver skin [7], with which our results agree on the skin's highly non-linear characteristics. Our results fit perfectly in line from what Wu has measured, with our average initial modulus 3.81 kPa, modulus at 25% strain 31.78 kPa, compared to 7.34 kPa initially and 37.97 kPa at 25% strain in pig skin. Further extending Wu's single-sample work, the multiple samples analyzed herein afford an analysis on how the variability of the thickness, stiffness and modulus were distributed, as noted above.

The behavior of the skin under compression studied herein are shown to be quite different from the skin in tension. Although the modulus at 5-10% strain in tension (5 kPa, [6]) is similar to that measured in compression (3.81 kPa, reported herein), the modulus at 20 - 30% strain in tension is increased by approximately two orders of magnitude (~6 MPa, [8]) as compared to that measured in compression (31.78 kPa, reported herein). In

particular, differences in the skin's response in compression as opposed to in tension become quite significant, for example in the case of modeling the skin to understand tactile perception where mechanoreceptors respond to skin deformation brought on by compressive mechanical stimuli [25].

Further work characterizing the skin in tensile and compressive regimes also requires more study of its time-dependent viscoelasticity, i.e., relaxation of the skin, following on prior work in tensile [14] and compressive [7] testing.

Finally, this work serves as an empirical data analysis effort. Further efforts may seek to extrapolate the uniaxial test data into a three dimensional finite element model. One could recreate such a model including the stress-strain curves from the parameters presented in results section (and supplementary data) and fit the curve to a hyperelastic strain energy function (e.g. 1st order Ogden form). For a fully descriptive three-dimensional hyperelastic-computational model, additional tests may be required, such as biaxial test and volumetric test.

2.4. Materials and Methods

Apparatus. A custom-built test machine was used to perform a uniaxial compression test of the flat, cylindrically cut skin samples. Overall, the test machine consists of a

vertically oriented load sled with a tip whose position is tracked by a laser and force by a load cell, Figure 2.2a. The compression tip is an aluminum plate, 3 mm thick and 2.54 cm diameter, connected by a rod to a load cell (Honeywell, Miniature Model 31, Columbus, OH) with full capacity of 2.45 N. The load cell is mounted to the motion controlled sled (motion controller: Newport, Model ESP300, Mountain View, CA; linear stage: Newport, Model ILS100). The tip compresses the skin specimens against a rigid plate that is parallel to the plate tip's surface. A laser displacement sensor (optoNCDT Model ILD 1402, Micro-Epsilon, Raleigh, NC) is used to measure displacement of the controlled movements, with resolution of 1 μm . Two classes of data are logged: force at the compression tip by the load cell and position from the laser sensor, both at a 1 kHz sampling frequency. A close-loop temperature system was integrated to control the temperature of the rigid plate using BASIC Stamp microcontroller module (Parallax Inc., Rocklin, CA).

Animals. All animal use was conducted according to the National Institutes of Health *Guide for the Care and Use of Laboratory Animals* and was approved by the Institutional Animal Care and Use Committee of Columbia University. The animal preparation and dissection protocol used are similar to previous study [25]. A total of 24 mice were sacrificed at ages ranging from 5.7 weeks to 34.3 weeks (Figure 2.1d). Four distinct groups were identified based on the hair cycle stages [24] and the mice were in at time of experiment, while the fifth group identified as mature group. Figure 2.1 shows

longitudinal cross-section histology figures of skin at mid-age of each group. Animals at 5.71 – 6.86 weeks were identified as in group Young Active (YA), at 9.00 – 10.29 weeks were identified as in group Young Resting (YR) according to literature [24]. Similarly, animals at 12.57 – 12.71 weeks were identified as Intermediate Active (IA), given the known start date of anagen phase as well as duration; 16.86 – 19.29 weeks were identified as Intermediate Resting (IR), by examining their skin flaps as they are known to be in a phase of mosaic hair cycling. 34.29 – 26.29 week animals were identified as group Mature (M).

Dissection. Once a skin flap from the mouse hind limb was dissected, skin punches were obtained using 6 mm diameter punch (Acuderm Inc., Ft. Lauderdale, FL) at sampling sites on distal end of the hind limb (distal), and the proximal end of the hind limb off, both off (OffNT) and on (NT) the nerve trunk, Figure 2.2b. These sampling sites were selected because they contain tactile end organs and appear to be categorically differentiable in terms of thickness and stiffness.

Skin Test Procedure. A total amount of 105 skin samples including 35 on distal, 34 on OffNT and 36 on NT are measured from the 24 animals. Among them, 4 are in the YA group, 9 are in the YR group, 3 are in the IA group, 2 are in the IR group and 6 are in the M group. Maximum indentation depths were determined by manually searching for an instantaneous reaction force around 2 N, which is on the approximate order to generate a

strain level of 25% similar to indentation in electrophysiological recordings [25]. The starting position of the compression tip was set to make sure that the tip was positioned above the skin surface, which is approximately 0.2 - 0.6 mm thick and are placed flat under the center of the tip. Displacement stimuli with a constant ramp-up speed of 10 $\mu\text{m/s}$ were loaded on the samples while the reaction force was logged. Droplets of synthetic interstitial fluid (SIF) were added via eye dropper to prevent skin from drying out. Pre-conditioning was skipped to minimize the variation caused by different strain levels at pre-conditioning between specimens [26]; the force trace from the first run was directly put into analysis.

Data Analysis. The raw force versus displacement data were first corrected for noise reduction and then converted into stress versus stretch change plots. First, the force trace was fitted using a cubic spline function for noise reduction and smoothing. Then the whole curve was compensated for the linear offset caused by reaction force from SIF – this is done by manually picking a range that is obviously before contact (i.e., 5-10 sec window before the force rises markedly, interval A in Figure 2.5a) and then offset the whole curve by the line fitted using this interval of data; force larger than the contact force threshold (F_T) of 0.01 N was treated as though the probe was in contact with the skin, point B in Figure 2.5a. The tip position at the contact time is then converted to skin thickness, Figure 5a. This same method had been adopted by Wu [7] and is more accurate than measurements by caliper [19] or dial micrometer [27].

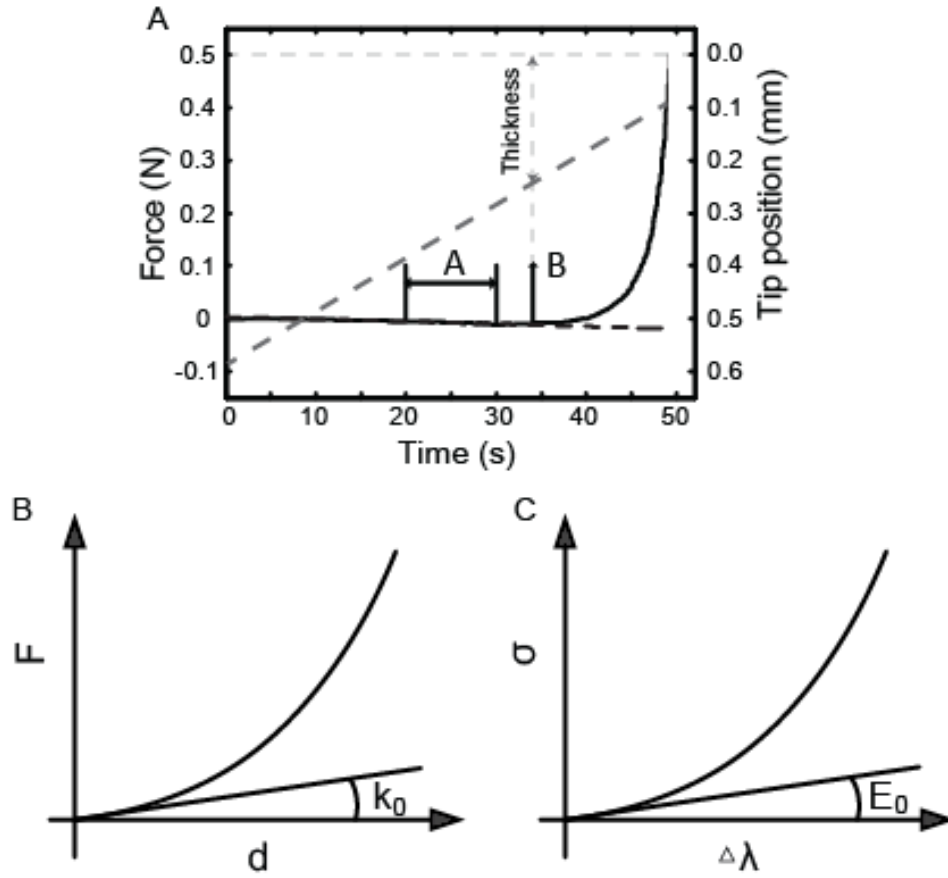


Figure 2.5 A: Example force and displacement vs. time plot. Illustration of SIF compensation on force traces, where interval A is the interval picked for curve-fitting in compensating error caused by SIF, and contact point B. Solid black line: force. Dashed grey line: displacement. Dashed black line: curve fit for SIF compensation. B: Schematic force vs. displacement plot. k_0 is the slope of the linear region, which indicates the initial stiffness of skin. C: Schematic stress vs. change in stretch plot. E_0 is the slope of the linear region, which indicates the initial Young's modulus of skin.

Secondly, we seek to convert the raw data of force vs. displacement to stress and stretch.

Stretch (λ) was calculated by deformed thickness (l) over original thickness (l_0) [28]:

$$\lambda = \frac{l}{l_0} , \quad (2.1)$$

In compression, for convenience in calculation the change in stretch is defined as:

$$\Delta\lambda = \lambda_0 - \lambda , \quad (2.2)$$

in this case $\lambda_0 = 1$. Similarly, compressive stress was defined positive and calculated using force over area (which was observed as approximately constant by a camera beneath during test runs).

Third, we seek to find appropriate form of functions and parameters to characterize the constitutive equations for skin material. After trying different candidates, we found the exponential function to fit the best. A single parameter curve fitting was used to fit both force vs. displacement curve and stress vs. stretch change curve. The force vs. displacement trace can be approximated using function in Equation (2.3), Figure 2.5b,

$$F = F_T(e^{pd} - 1), \quad (2.3)$$

where F is the reaction force at the compression tip, F_T denotes the contact force threshold, the exponential linear coefficient p indicates the non-linear stiffness of the skin (referred to as stiffness exponent) and $d = l_0 - l$ represents displacement into skin, which is calculated from the position of the compression tip at the time when the force transducer reading rises above the pre-set contact threshold F_T .

Similarly, Equation (4), was used to approximate the stress vs. change in stretch curve, Figure 5c,

$$\sigma = \sigma_T(e^{q\Delta\lambda} - 1), \quad (2.4)$$

where σ_T is the stress value at contact threshold and is obtained by F_T/A , A denotes surface area of the specimen, $A = \pi r^2$, and r is the radius of the sample ($r = 3$ mm), the

exponential linear coefficient q indicates the hyperelastic modulus of the specimen (referred to as modulus exponent), σ represents Cauchy stress obtained by F/A and $\Delta\lambda$ represents stretch change, with the reference length of the skin thickness.

Two important derivations from the formula above are used in the analysis effort. (Detailed derivations are listed in the Appendix A.)

1) Initial stiffness and initial modulus of skin

$$k_0 = pF_T \quad (2.5)$$

$$E_0 = q\sigma_T \quad (2.6)$$

where k_0 and E_0 denote the initial stiffness and initial Young's modulus of the skin. These two parameters sufficiently described the material elasticity under small deformations; however since the skin is highly compliant and hyperelastic, these two parameters are not the best parameters characterizing the skin given compression greater than approximately 5%, Figure 2.5c, 2.5d. Eqn. (2.5 – 2.6) can be acquired by calculating partial derivative of Eqn. (2.3) and Eqn. (2.4) with regard to d or $\Delta\lambda$ at value 0.

2) The relationship between stiffness exponent (parameter p) and modulus exponent (parameter q)

$$p = \frac{q}{l_0} \quad (2.7)$$

Recall that l_0 is the thickness of the skin. Eqn. (2.7) can be derived by solving Eqn. (2.1 – 2.4) together.

Curve fitting of force vs. displacement and stress vs. stretch change is performed via MATLAB (Mathworks, 2011b, Natick, MA). The average resultant R^2 values for the all the fitting is 0.98.

3. Analysis on Skin Viscoelasticity

3.1. Introduction

The skin is a complex structure that consists of unique layers of epidermal, dermal and subcutaneous fat [13] which overlay muscle tissue and bone. Mechanically, the skin is a non-linear, hyperelastic material [7] that exhibits time-dependent viscoelastic relaxation and creep, which are behaviors tied to the properties of the elastin, proteoglycan, collagen and interstitial fluid [14], [15]. As well, embedded collagen bundles give rise to greater forces in tension than compression [16]. The geometry and characteristics of the interfaces between individual skin layers are often undulating and tied tightly together, the structure and function of which vary between skin sites [17], as does overall thickness. At present, a better understanding of the skin's mechanical properties is sought by researchers in dermatology, studying touch interfaces and treatment for syndromes such as bed sores and diabetic foot. However, the measurement of the skin's many dimensions remains a complex undertaking.

The skin's mechanics have been measured using uniaxial and biaxial tension tests, in addition to uniaxial compression, torque loading, and indentation [9]. The latter two are indirect methods, which for soft materials tend to generate highly non-linear stress fields, therefore making it difficult to calculate constitutive laws relating material stress to strain. The former two more readily afford constitutive models and importantly material quantification in an absolute, as compared to comparative fashion. Most typically, the tensile regimes are used. For example, in uniaxial tension tests with human cadaver tissue, the stress-strain curve was found to be linear under small deformations, non-linear at intermediate strains and again linear at large levels of strain [9]. Further, uniaxial tension tests have investigated the time-dependent creep and relaxation of the skin, showing that rat dorsal skin, under tension, is quasi-linear viscoelastic [14]. Others have conducted bi-axial tension tests, both in rats [18] and human cadavers [19]. Comparatively in compression, many fewer tests have been conducted. This is due in part to experimental difficulties and the availability of predefined material models. In one notable case, compression loading was done with pigskin, considering the skin's non-linearity and viscoelasticity, though done on a single specimen basis with small ($< 10\%$) deformation [7].

The skin behaves dramatically different in tension than in compression. While in small deformation the elastin plays a role in either tension or compression, in larger deformation, the collagen fibers pull tight under tension for an increase in force whereas

under compression they play little to no role. As a consequence, although the modulus at 5-10% strain in tension (5 kPa, [6]) is similar to that measured in compression (7.34 kPa, [7]), the modulus at 20 - 30% strain in tension is increased by approximately two orders of magnitude (~6 MPa, [8]) as compared to that measured in compression (37.97 kPa, [7]). We know even less as to how viscoelasticity in tensile and compressive regimes varies.

The specific gap in the knowledge base is that there is little existing data on the viscoelasticity of the skin, especially done in a state of compression.

The work herein addresses this gap by use of compressive uniaxial tests on freshly excised mouse skin across a population of skin samples. In specific, the data were analyzed according to two research questions:

- (1) Is skin viscoelasticity coupled with loading conditions, specifically loading velocity?
- (2) How is skin viscoelasticity tied to case-by-case factors of the harvested sample, specifically thickness?

The methods utilize controlled displacement, linearly ramped into the skin surface, at various velocities of 0.01, 1 and 3.63 mm/s to collect time-force-displacement data from which we generate material parameters in the commonly used quasilinear viscoelasticity model. Also calculated was skin thickness, using a new method based on contact force,

which contrasts with traditional methods that utilize calipers and glass slides [19]. The measured specimens were comprised of 98 skin samples freshly excised from 23 mice, ranging in age 5.71 – 34.29 weeks, and from skin sites on hind limb.

3.2. Methods

Apparatus. A custom-built test machine was built to perform uniaxial compression of flat cylindrically cut skin samples, as described elsewhere [29]. The test machine's components include a compression plate of aluminum (3 mm thick and 2.54 cm dia.) attached to a vertical load sled, which is driven by a motion controller (motion controller: Newport, Model ESP300, Mountain View, CA; linear stage: Newport, Model ILS100, Figure 2.2A and B). Reaction force at the compression tip is measured by a loadcell (Honeywell, Miniature Model 31, Columbus, OH) with full capacity of 2.45 N mounted between the tip and vertical load sled, and its position was tracked by a laser displacement sensor (optoNCDT Model ILD 1402, Micro-Epsilon, Raleigh, NC) with a resolution of 1 μm . Both force and displacement were sampled at 1 kHz. The tip compresses the skin specimens against a rigid plate that is parallel to the plate tip's surface, with a closed-loop control system integrated to maintain temperature of 32 Celsius degrees, using a BASIC Stamp microcontroller (Parallax Inc., Rocklin, CA) and associated electronic transistors and heating elements.

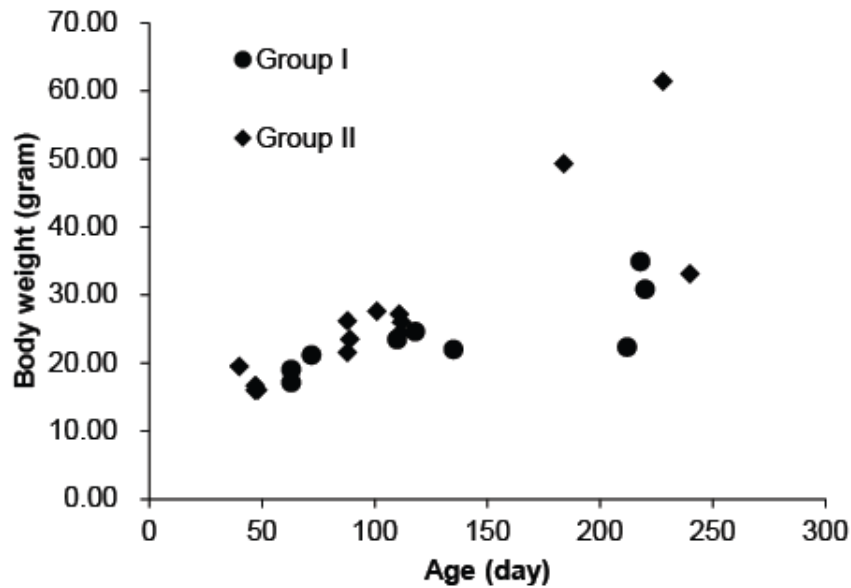


Figure 3.1 Plot of body weight vs. age for 23 animals. Dots denote animals in Group I (tested under 3.63 mm/s and 0.01 mm/s), diamonds denote animals in Group II (tested under 1 mm/s).

Animals and dissection. All animal use was conducted according to the National Institutes of Health *Guide for the Care and Use of Laboratory Animals* and was approved by the Institutional Animal Care and Use Committee of Columbia University. The animal preparation and dissection protocol used are similar to prior work [25]. A total of 23 mice were sacrificed at ages ranging from 5.71 weeks to 34.29 weeks, body weight ranging from 15.94 grams to 61.39 grams (Figure 3.1C). Figure 3.2.2 shows longitudinal cross-section histology figures of skin at three ages across the span, namely 9.14, 15.71 and 31.29 weeks. Skin samples were obtained using 6 mm diameter punch (Acuderm Inc., Ft. Lauderdale, FL) after the skin flap from the mouse hind limb was dissected. Three sampling sites were chosen at distal end of the hind limb (distal), and the proximal end of

the hind limb off, both off (OffNT) and on (NT) the nerve trunk (Figure 3.2.1B) because they contain tactile end organs and appear to be categorically differentiable in terms of thickness. A total of 98 skin samples including 33 on distal, 32 on OffNT and 33 on NT were harvested from the 23 animals.

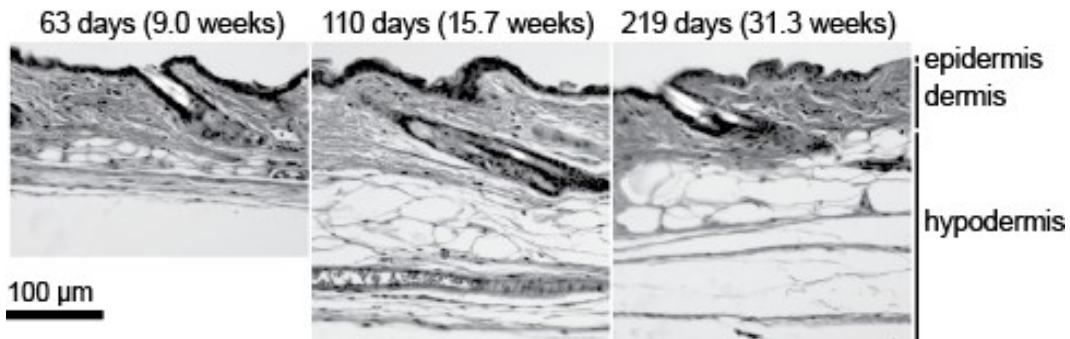


Figure 3.2 Longitudinal cross-section histology images taken from sampling sites.

Skin Test Procedure. At first, maximum indentation depths were determined by manually searching for an instantaneous reaction force around 2 N, which is of approximate magnitude to generate a level of strain of 25%, similar to indentation in electrophysiological studies [25]. The starting position of the tip was set to make sure it was positioned above the flat skin surface, which is approximately 0.2 - 0.6 mm thick. The indentation was displacement-controlled, with a ramp-up phase at a controlled velocity, a hold phase at the maximum load position for 6 seconds, and an unloading phase of the same velocity as the ramp-up. The stimuli were repeated 10 times, with the 6th run being analyzed and other runs as pre-conditioning runs to minimize the variance due to stress history [26]. The reaction force at the tip was logged by the loadcell and tip

position by laser displacement sensor. Three velocities were adopted: slow = 0.01 mm/s and medium = 1 mm/s, both commanded and achieved; fast = 100 mm/s commanded and approximately 3.63 mm/s achieved. Note that at the highest rate of ramp-up the indenter was unable to achieve the desired velocity. Skin samples were randomly divided into two groups: 54 samples in group I and the other 44 in group II. For group II, only medium ramp velocities were used, while for group I the ramp velocity was first 0.1 mm/s and then repeated at 3.63 mm/s. Synthetic interstitial fluid (SIF) were added via eye dropper to prevent the drying out of the skin.

Constitutive modeling. Hyper- and viscoelastic models have been adopted to fit the behavior of the experimental data, as previous efforts [7], [29] have shown that skin under compression is hyper-viscoelastic. Given the test is uniaxial, the model herein only considers the one-dimensional situation. According to quasilinear theory [30], a convolution integral is used to calculate stress from strain data,

$$\sigma(t) = \int_{-\infty}^t G(t - t') \frac{\partial \sigma_e(\lambda_{t'})}{\partial t'} dt', \quad (3.1)$$

where t and λ denote time and stretch at any given moment t . The instantaneous elastic function of material is $\sigma_e(\lambda)$, where herein we utilized a 1st-order Ogden form of the hyperelastic strain energy function [28],

$$\sigma_e(\lambda) = \frac{2\mu}{\alpha} (\lambda^\alpha - \lambda^{-\frac{\alpha}{2}}), \quad (3.2)$$

with μ and α being the material constants, μ also known as instantaneous elastic modulus.

$G(t)$ is defined as the reduced relaxation function, and is in the form of a two-term Prony

series,

$$G(t) = \sum_{i=1}^2 G_i e^{-\frac{t}{\tau_i}} + G_{\infty}, \quad (3.3)$$

where τ_i are the time constants associated with weights G_i , and G_{∞} is the residual weight at the steady state. At time $t = 0$ the value of $G(t)$ was defined as unity,

$$\sum_{i=1}^2 G_i + G_{\infty} = 1. \quad (3.4)$$

Fitting experimental data to constitutive model. To attain the parameters of the constitutive model, we fit the model to the stress time curves calculated from the experimental data. The contact time of indenter tip to specimen surface, from the experimental data, was determined at the moment when reaction force on the tip exceeds 0.01 N. After that, the thickness of the skin sample was taken as distance from the tip to the rigid plate at the contact time, thereby the stretch was calculated by dividing deformed thickness over original thickness. Recorded experiment force data were converted to stress values by dividing force over area, which is the area of the punch, a six mm diameter circle. Note that the area was observed to be constant, according to video camera surveillance of trial-runs that indicated the skin area did not change significantly over the course of a testing cycle. The algorithm developed in Eqn. (3.1) was then fit to the stress-time and stretch-time measurements (Figure 3.3).

All function fits were performed via MATLAB (Mathworks, 2011b, Natick, MA). The average resultant R^2 values for the fitted model are 0.96.

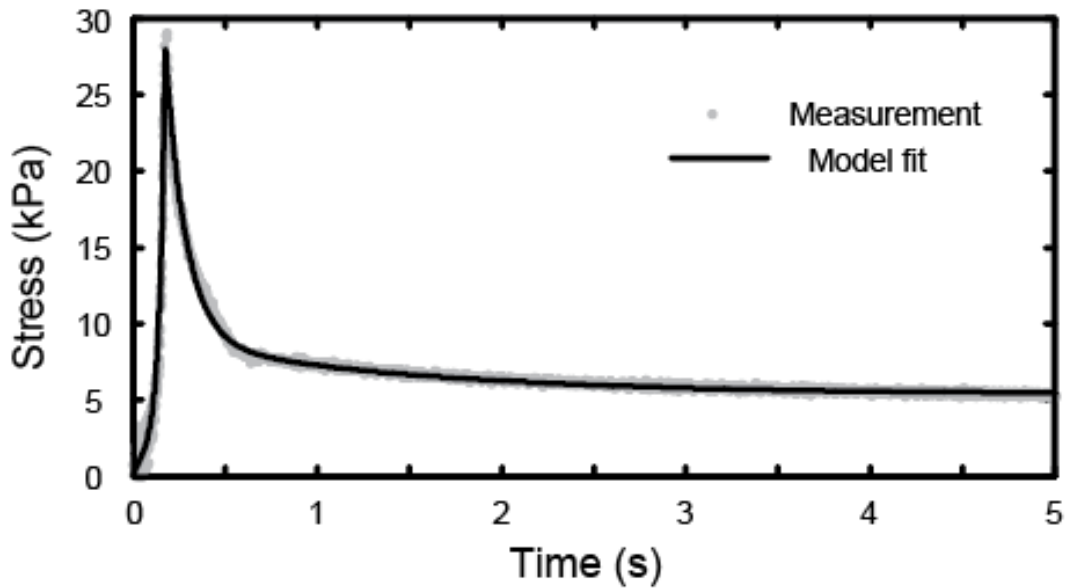


Figure 3.3 A typical fit of the constitutive model to the experimental stress-time curves, under the medium ramp velocity of 1 mm/s.

3.3. Results

Two main findings emerge from this study. The viscoelastic properties of the mouse skin specimens under compression are dependent on the loading velocity and thickness of the specimen.

Dependency of viscoelasticity on rate of the loading process. As loading velocity increases, the same magnitude of relaxation takes place at significantly shorter time constants. Comparison within group I at different ramping velocities (slow as 0.01 mm/s,

fast as 3.63 mm/s) shows that the rate of loading significantly impacts both time constants (Figure 3.4A and 3.4B). The time constants under fast loading are significantly smaller compared to slow loading (p-value < 0.05), while the values of the weights (G_i) from the reduced relaxation function are not significantly different (p-value > 0.6 for G_1 and G_∞ , p-value > 0.05 for G_2), as shown in Figure 3.4C, D and E. The instantaneous elastic modulus μ in Eqn. (3.2) also increases from 8387.10 ± 11.77 Pa under 0.01 mm/s, to 14097.59 ± 6019.63 Pa under 3.63 mm/s.

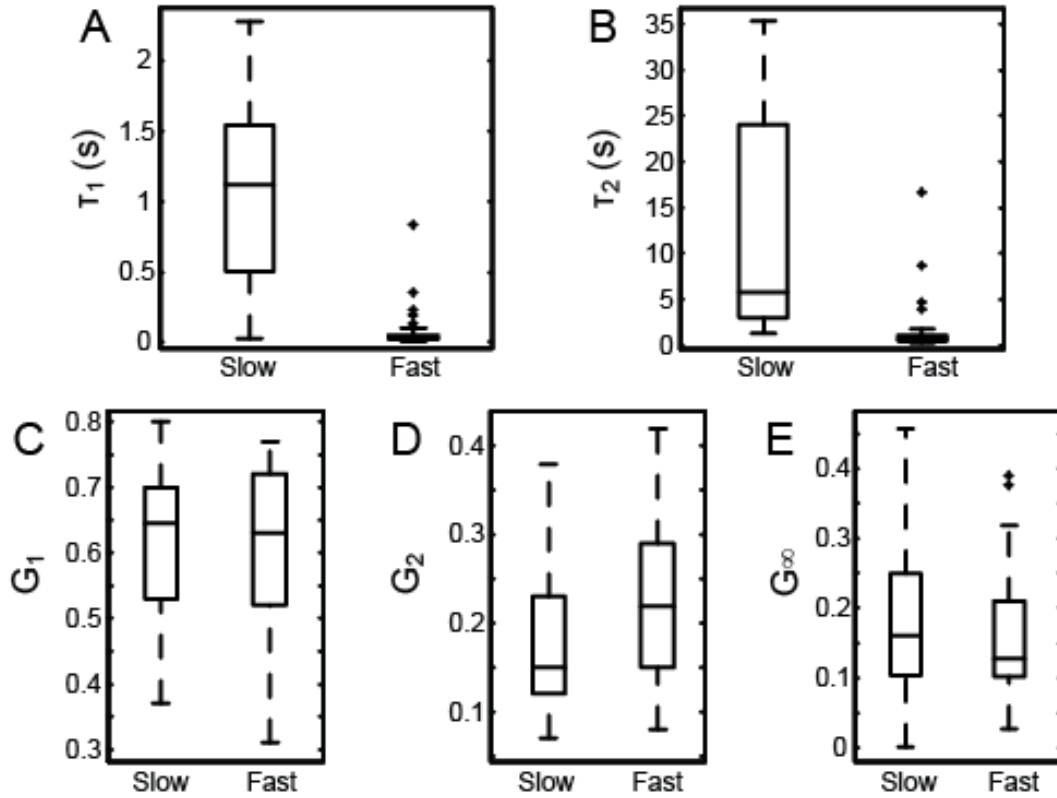


Figure 3.4 A and B: Boxplots of time constants as ramp velocity varies from X mm/s to Y mm/s. C,D and E: Boxplots of weights (G_i) from the reduced relaxation function at the two ramp velocities.

Dependency of viscoelasticity of thickness of specimen. For thinner skin specimens,

greater relaxation is observed over the identical time constants. Values of the weights (G_i) from the reduced relaxation function are dependent on the thickness of tissue, according to the analysis within group II. G_1 , G_2 are negatively correlated and G_∞ is positively correlated with thickness of skin, all p -value < 0.01 (Figure 3.5). No significant correlation has been found with regard to either of the time constants ($|r| < 0.3$, p -value > 0.05) for both τ_1 and τ_2 . Linear regressions with thickness as predictor and G_i values as objective state that G_1 drops from 0.76 to 0.50, G_2 drops from 0.19 to 0.11, and G_∞ increases from 0.05 to 0.40, as thickness goes from 171.34 μm to 607.31 μm .

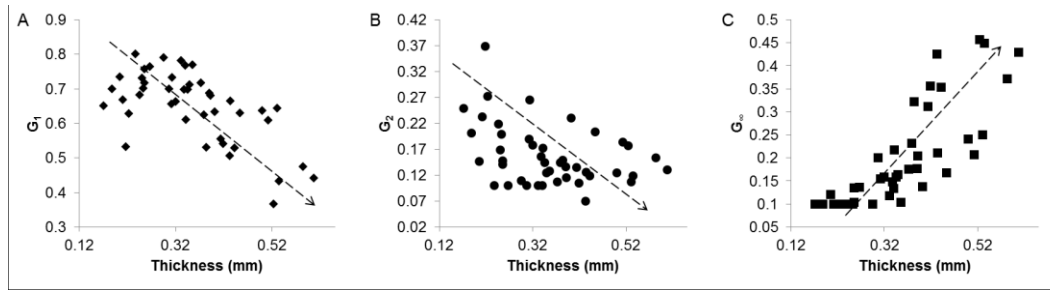


Figure 3.5 Plot of weights in reduced relaxation function vs. specimen thickness. A: G_1 vs. thickness ($r = -0.64$, $p < 0.01$); B: G_2 vs. thickness ($r = -0.38$, $p < 0.01$); C: G_∞ vs. thickness ($r = 0.79$, $p < 0.01$).

3.4. Discussion

This work shows, presumably for the first time with skin in compression, that freshly excised skin exhibits viscoelastic relaxation dependent both on the delivery of the stimulus (loading velocity) and innate skin properties (thickness of the skin). More

specifically, we found that 1) as loading velocity increases, the same magnitude of relaxation takes place over a significantly shorter time constant; 2) for thinner skin specimens, greater relaxation is observed over the same time constant. These are important issues revealed in traditional quasilinear viscoelastic model when applied to skin materials, because existing constitutive models do not include factors of levels of strain and loading velocity.

We believe the dependency of loading rate is due to the following cause. During the course of the skin's relaxation, the free flow of interstitial fluid keeps taking place proportionally. As interstitial fluid plays an important role in skin's viscoelasticity, the change of its amount and how the fluid is distributed within the tissue causes different relaxation behaviors. The increase of instantaneous modulus observed as the rate of loading increases may tend to agree, as well, with electrophysiological recordings from tactile mechanoreceptors where increased probe velocity yields higher firing rates from slowly adapting type I afferents [31], [32], though the neuron itself may play a role apart from the skin's response. This result may suggest a need to control loading velocity in electrophysiological experiments. Also, since thicker skin relaxes faster, work herein also predicts that the neural response from slowly adapting type I afferents in thicker skins may have the tendency to adapt their firing rates faster to held stimuli.

Impact of skin thickness on its relaxation behavior. We observe that for thinner skin

specimens, a greater amount of relaxation is observed over the same time course. One might expect the same characteristics of relaxation of the skin regardless of thickness. However, that we see this may potentially be due to the various layers that are grouped together. In particular, there may be a non-proportional growth of epidermal, dermal and hypodermal layers as skin thickens. For example, when skin thickness increases by 10%, the epidermal, dermal and hypodermal tissue might not each thicken by 10%, rather the hypodermis might grow 30% while epidermis does not grow at all, though at present this has not been observed. Large changes in the G_i values as well as thickness indicate a large variation in skin viscoelastic properties, though at same time constants. This goes together with previous analysis, that skin thickness was identified as a key parameter of its mechanical properties [29], which is a synthetic representation of how other factors of age, skin site, hair cycle stage, body weight and maturity impact skin mechanical properties in hyperelastic regime.

Comparison to prior tests of skin compression and tension. The mean result herein is comparable to prior measurements on pig skin [7], with time constants at the same order of magnitude (0.10 and 2.05 seconds herein, compared to 0.57 and 9.47 seconds on pig skin). However, if we compare the reduced relaxation functions of skin, under compression, together with those of rat skin, under tension [16], the compression curves are clearly distinguishable by their significantly smaller residual value with time (Figure 3.6).

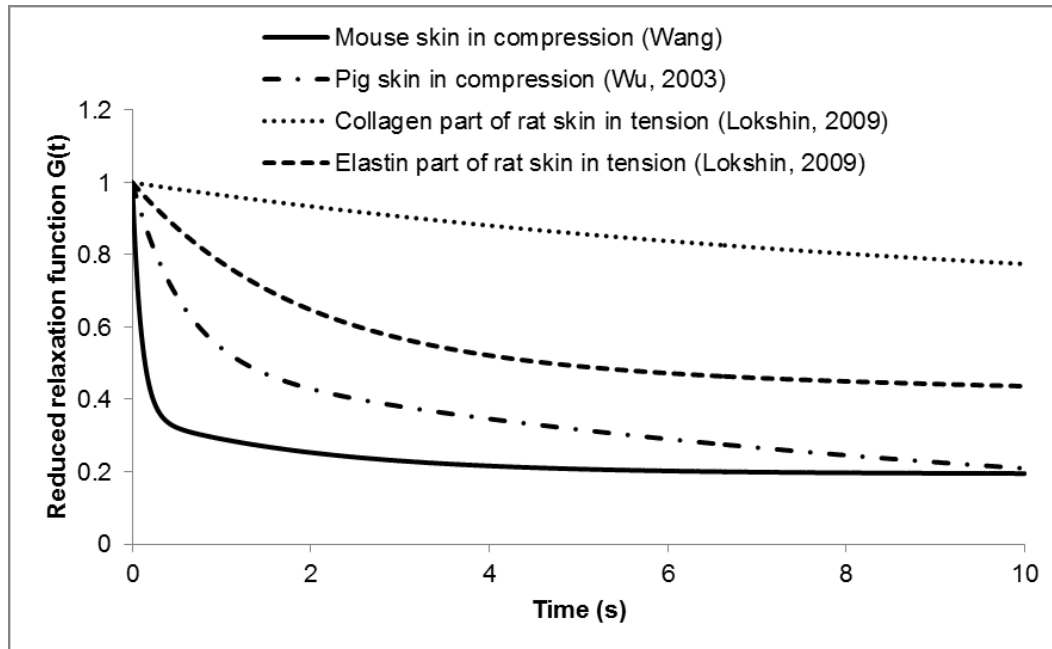


Figure 3.6 Comparison of reduced relaxation functions between compression and tension and between compression in the mice, rat and pig, where in the mouse we measured 98 samples and calculated the average.

Another key difference herein compared to prior work is the use of skin from the hindlimb, instead of the more commonly used dorsal skin of the back. While dorsal skin is more accessible and continuous, skin near mechanoreceptive endings is more suited to studying touch.

4. Impact of Skin Properties on SAI

4.1. Introduction

Our tactile perception of spatial curves, edges, and varying stimulus magnitudes is essential to daily interactions. In mammals, these functions are supported by four classes of mechanosensitive afferents, including slowly adapting type I (SAI) afferents which innervate Merkel cell-neurite complexes [1], [33]. Tactile perception is typically studied at one of two levels: neurophysiological recordings of action potentials from single afferents and psychophysical experiments of human perception that measure stimulus thresholds and difference discrimination [34]. To close the gap between these two levels, modeling efforts have sought to mimic skin mechanics as well as neuronal dynamics.

Spanning neurophysiological and psychophysical experiments as well as modeling efforts, the indentation of mechanical stimuli into the skin has been controlled both by displacement and force. A review of the literature reveals that psychophysical experiments generally use force control, whether considering grating orientation [35] sphere size [36], or spatial anisotropy [37]. There are two potential reasons for this preference. First, investigations of grasp [38] indicate that people systematically control their load and grip forces during dexterous manipulation. Second, during active touch, it is much easier to control one's applied force than displacement, especially when visual cues are eliminated. By contrast, displacement control is typically used in modeling

studies of skin mechanics, including continuum mechanics [12], [39] and finite element models [3], [11], [40]. This may be due to the fact that most validate to surface deflection [41], based on experiments that used prescribed displacements. In the case of neurophysiological studies, the modes of control have been employed about equally, with displacement [25], [42] and force [43], [44] used in both animal and human studies.

The impact of stimulus delivery on variability of neural and behavioral responses has not been previously considered. At the same time, we know that the skin's mechanical properties vary not only with age [9], [10], [45], but also intuitively with size, weight, and occupation. Given such variance, we hypothesize that stimulus control by force might better equalize between-subject responses. Specifically, if skin thickness changes while elasticity remains the same, a displacement-controlled stimulus might generate much greater local stresses in thinner skin due to greater strain exerted at the skin's surface. Such understanding is relevant in the design of the next generation of tactile interfaces [46].

This study examines, informed by compressive measurements of mouse skin and use of solid mechanics models, the predicted variation of firing rate of SAI afferents under stimulus control by both displacement and force. First, using uniaxial compression, we measured the skin's thickness and hyper-viscoelasticity for five skin samples to determine the variation in properties. Second, we built and validated a numerical model (with finite

elements to represent skin and an empirically fitted equation for neural firing) for a single SAI afferent to predict firing rates. Third, we performed exploratory numerical experiments whereby the skin thickness in the model was varied over the measured range to determine its impact on predicted firing rate under both modes of control.

4.2. Methods

4.2.1. Mouse Skin Measurements

Animals and dissection. All animal use was conducted according to the National Institutes of Health Guide for the Care and Use of Laboratory Animals and was approved by the Institutional Animal Care and Use Committee of Columbia University. Animal preparation and dissection was performed as previously reported [25]. Five skin samples were harvested from a total of four mice (Table 4.1), and numbered as #0 for model fitting and validation, #1–#4 for simulation. Once a skin specimen from the mouse hind limb was dissected, skin punches were obtained using 6-mm diameter punch (Acuderm Inc., Ft. Lauderdale, FL) at sampling sites on the hind limb as these sites contain tactile end organs.

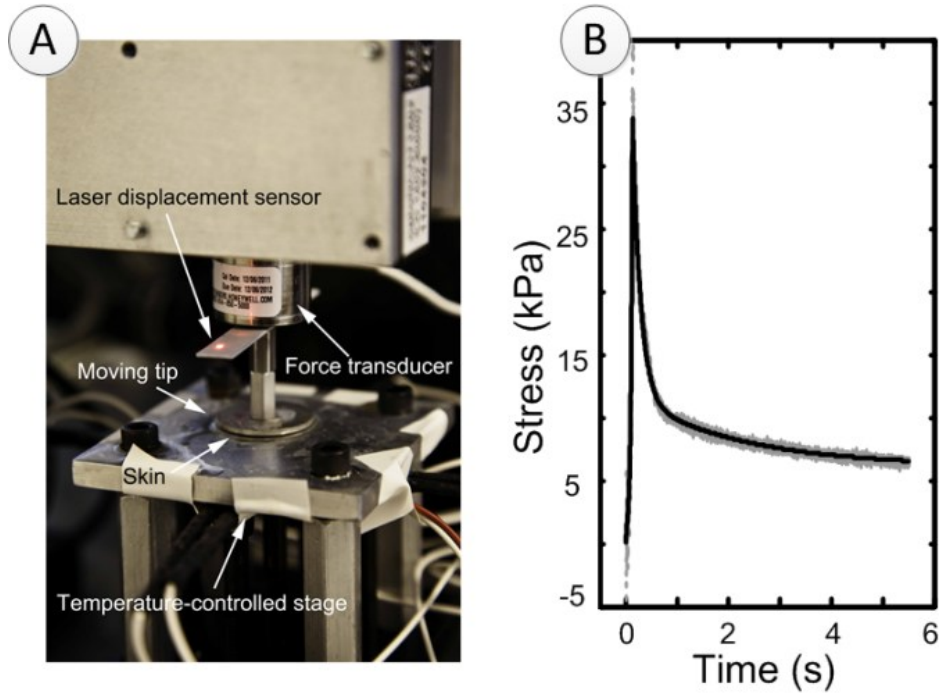


Figure 4.1 A: Uniaxial compression test machine. B: Example of recorded stress-time data (grey dots) and model fit (black line).

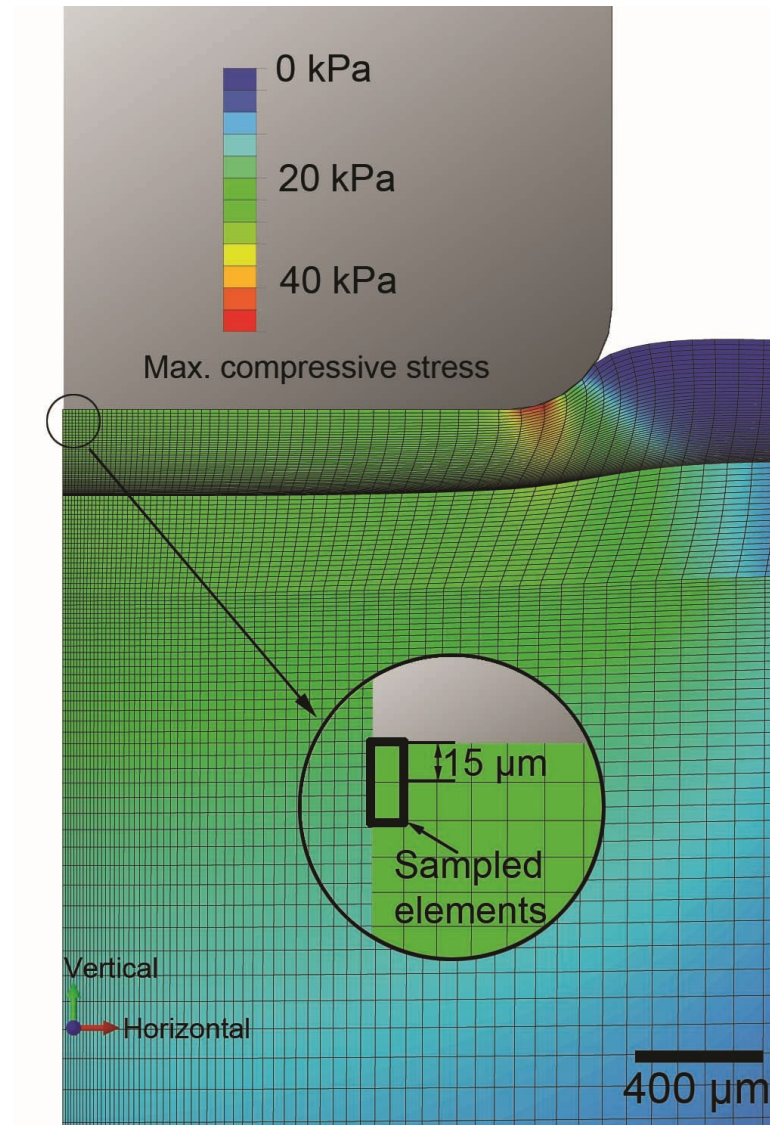


Figure 4.2 Contour map of maximum compressive stress in the FE model upon indentation by a 3.42 mm diameter cylinder. The highlighted elements represent locations of the tactile end organs of the SAI afferent.

Apparatus. A custom-built test machine was used to perform uniaxial compression tests of skin samples (Figure 4.1). Overall, the test instrumentation consisted of a vertically oriented load sled with a tip, whose position was tracked by a laser and force by a load cell. The compression tip was an aluminum plate, 3 mm thick and 2.54 cm diameter,

connected by a rod to the load cell (Honeywell, Miniature Model 31, Columbus, OH) with full capacity of 2.45 N. The load cell was mounted to the motion controlled sled (motion controller: Newport, Model ESP300, Mountain View, CA; linear stage: Newport, Model ILS100). The tip compressed the skin specimens against a rigid plate parallel to the plate tip's surface. A laser displacement sensor (optoNCDT Model ILD 1402, Micro-Epsilon, Raleigh, NC) measured displacement of the controlled movements, with resolution of 1 μm . Two classes of data were logged: force at the compression tip by the load cell and position from the laser sensor, both at a 1 kHz sampling frequency. A closed-loop temperature system was integrated to control the temperature of the rigid plate using BASIC Stamp microcontroller module (Parallax Inc., Rocklin, CA).

Skin Test Procedure. Maximum indentation depths were determined by manually searching for an instantaneous reaction force around 2 N, which is on the approximate order to generate a strain level of 25% similar to indentation in electrophysiological recordings [25]. The starting position of the compression tip was set to make sure that the tip was positioned above the skin surface. Skin punches were approximately 0.2–0.6 mm thick and were placed flat under the center of the tip. Displacement stimuli with a constant ramp-up speed of 1 mm/s were loaded on the samples while the reaction force was logged. Droplets of synthetic interstitial fluid (SIF) were added via eye dropper to prevent skin from drying out. Experiment temperature was set at 32 Celsius degrees to match *in vivo* skin temperatures. Five pre-conditioning runs were performed; force traces

from the 6th run were analyzed.

Parameter fitting. The 1st order Ogden type of strain energy function was used for instantaneous hyperelasticity [28], whereas the quasi-linear viscoelastic model [47] with 2-term Prony series was used for viscoelasticity. Note that parameter μ_1 is fixed during fitting. The fitting is done with Matlab (MathWorks, Natick, MA).

4.2.2. Numerical Model

Two sub-models constituted the numerical model: skin mechanics sub-model (FE model), and the neural transduction sub-model.

Construction of FE model. The commercial software ABAQUS (Dassault Systèmes, Vélizy-Villacoublay, France) was used for FE modeling. An axisymmetric finite element model (Figure 4.2) with hyper- and visco-elastic material properties was developed to mimic the reactions of the skin properties given indentation techniques of ramp-and-hold stimuli in both displacement and force control. The model comprised ~14,000 elements (element type CAX4RH) and three layers to match neurophysiological recordings: top layer, skin; middle layer, nylon perfusion wick; and a bottom substrate of silicone elastomer. Silicone elastomer, often Sylgard, is used in electrophysiological recordings to mimic muscle tissue, and nylon serves to improve SIF circulation [25], [48]. Thicknesses

and mechanical properties of skin were set according to measured values on samples by uniaxial compression test by a rigid cylindrical indenter tip (3.42 mm diameter and with 0.32 mm radius edge-rounded fillet, based on the one used in electrophysiological recordings), and those of Sylgard and nylon were obtained from inverse FE model fitting with indentations by a spherical indenter tip (3.5 mm diameter). The surface interaction between indenter and skin was set as frictionless. Maximum compressive stresses [39] at the center top element and the immediate element below were extracted and averaged, since the intersection of the two elements was at 15 μm below skin surface which approximates the locations of Merkel cell-neurite complexes.

Electrophysiological recording data and FE model validation. Previously published electrophysiological recordings [31] were used to compare and validate the numerical model. In the experiment, ramp-and-hold displacement stimuli were delivered to skin, with nylon and Sylgard as substrate. Ramp durations varied between 100–400 ms, and the duration of the sustained load was 5 s. Two distinct phases were identified [49]: a) dynamic ramp phase (also noted as dynamic phase), defined from $t=0$ s to the time when the peak force was achieved; b) sustained hold phase (also noted as static phase), defined from $t=2$ to 5 s. For model validation, predicted force traces were compared with those experimentally recorded.

Neural transduction sub-model fitting and validation. Absolute values of stress and stress rate (derivative of stress with respect to time) were averaged within span of dynamic and static phases individually. Then, a linear regression (Eqn. 5.1) was performed with independent variables as absolute values of averaged stress and stress rate, and dependent variable as average firing rate (inverse of average inter-spike intervals), respectively in dynamic and static phases. Note that there was no constant term in this regression. The regression equation is:

$$\bar{f} = k_1|\bar{\sigma}| + k_2|\bar{\dot{\sigma}}| \quad (5.1)$$

where \bar{f} denotes average firing rate, $|\bar{\sigma}|$ denotes the absolute value of average stress, $|\bar{\dot{\sigma}}|$ denotes the absolute value of average stress rate, and k_1, k_2 are stress and stress rate coefficients to be calculated from the regression.

4.2.3. Exploratory Numerical Experiments

To systematically explore how changes in skin thickness might impact firing rate under both displacement and force control, we performed four additional experiments varying values for thickness as well as material properties. For each thickness of model, two stimulus types were applied: a) for displacement-controlled stimuli, the load was 0.19 mm with linear ramp over 148.89 ms; b) for force-controlled stimuli, the load was 0.2 N with linear ramp over 148.89 ms. These magnitude and rise time were set to be 1)

consistent with electrophysiological recording set-up, 2) comparable between two stimuli types. For all model simulations, parameters of the neural transduction function were held constant.

4.3. Results

Material measurements. The result of the parameter fits to the skin measurements are listed in Table 5.1, as well as properties of nylon and Sylgard. The average R^2 for skin parameter fitting is 0.97. Note that the variation in skin thicknesses between #1–#4 (CV=0.36) is more pronounced than in elasticity parameter α_1 (CV=0.04).

Table 5.1 Material parameters of the different skin specimens, as well as Sylgard and nylon in skin-nerve preparation.

Material	Age (days)	Thickness (μm)	Hyper-elastic (Instantaneous)		Visco-elastic (Prony series)	
			Type	Parameters	τ values	g values
Skin #0	101	325.80	1 st order Ogden	$\mu_1=9188.5 \text{ Pa}$, $\alpha_1=16.88$	$\tau_1=0.16 \text{ s}$, $\tau_2=2.14 \text{ s}$	$g_1=0.70$, $g_2=0.15$
Nylon	-	338.80	1 st order Ogden	$\mu_1=42368 \text{ Pa}$, $\alpha_1=9.00$	$\tau_1=0.25 \text{ s}$, $\tau_2=5.00 \text{ s}$	$g_1=0.48$, $g_2=0.02$
Sylgard	-	10134.8	Neo-Hookean	$C10=105169 \text{ Pa}$	$\tau_1=0.7$	$g_1=0.03$
Skin #1	101	211.57	1 st order Ogden	$\mu_1=9188.5 \text{ Pa}$, $\alpha_1=16.49$	$\tau_1=0.09 \text{ s}$, $\tau_2=0.73 \text{ s}$	$g_1=0.68$, $g_2=0.25$
Skin #2	111	341.67	1 st order Ogden	$\mu_1=9188.5 \text{ Pa}$, $\alpha_1=15.83$	$\tau_1=0.11 \text{ s}$, $\tau_2=1.13 \text{ s}$	$g_1=0.61$, $g_2=0.17$
Skin #3	240	454.01	1 st order Ogden	$\mu_1=9188.5 \text{ Pa}$, $\alpha_1=15.04$	$\tau_1=0.02 \text{ s}$, $\tau_2=0.33 \text{ s}$	$g_1=0.65$, $g_2=0.20$
Skin #4	228	530.60	1 st order Ogden	$\mu_1=9188.5 \text{ Pa}$, $\alpha_1=15.85$	$\tau_1=0.11 \text{ s}$, $\tau_2=1.58 \text{ s}$	$g_1=0.64$, $g_2=0.11$

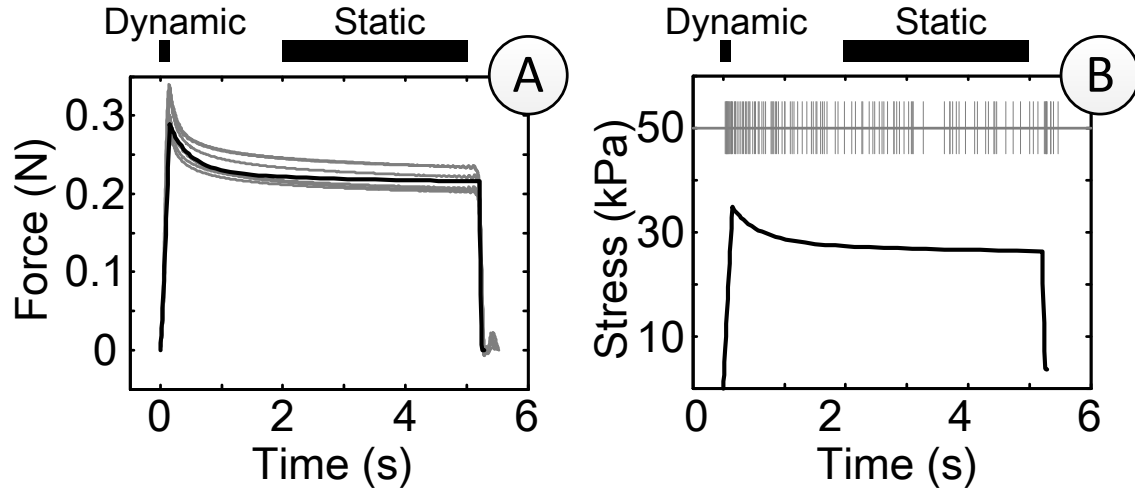


Figure 4.3. A: FE model prediction (black) and recorded (gray) force. B: Model predicted maximum compressive stress at receptor location (black solid line) compared with recorded SAI action potential trains (gray vertical dashes).

Numerical model fit and validation. Linear regression gave values for stress coefficient $k_1=0.490$ Hz/kPa, and stress rate coefficient $k_2=0.334$ Hz/(kPa \cdot s $^{-1}$). Both independent variables are significant ($P<10^{-4}$), and the R^2 for the regression is 0.995. This model was validated by a) comparing predicted and recorded force traces (Figure 4.3A); b) comparing model output with recorded firing rate (Figure 4.3B) in dynamic and static phases (Figure 4.4A and B) respectively.

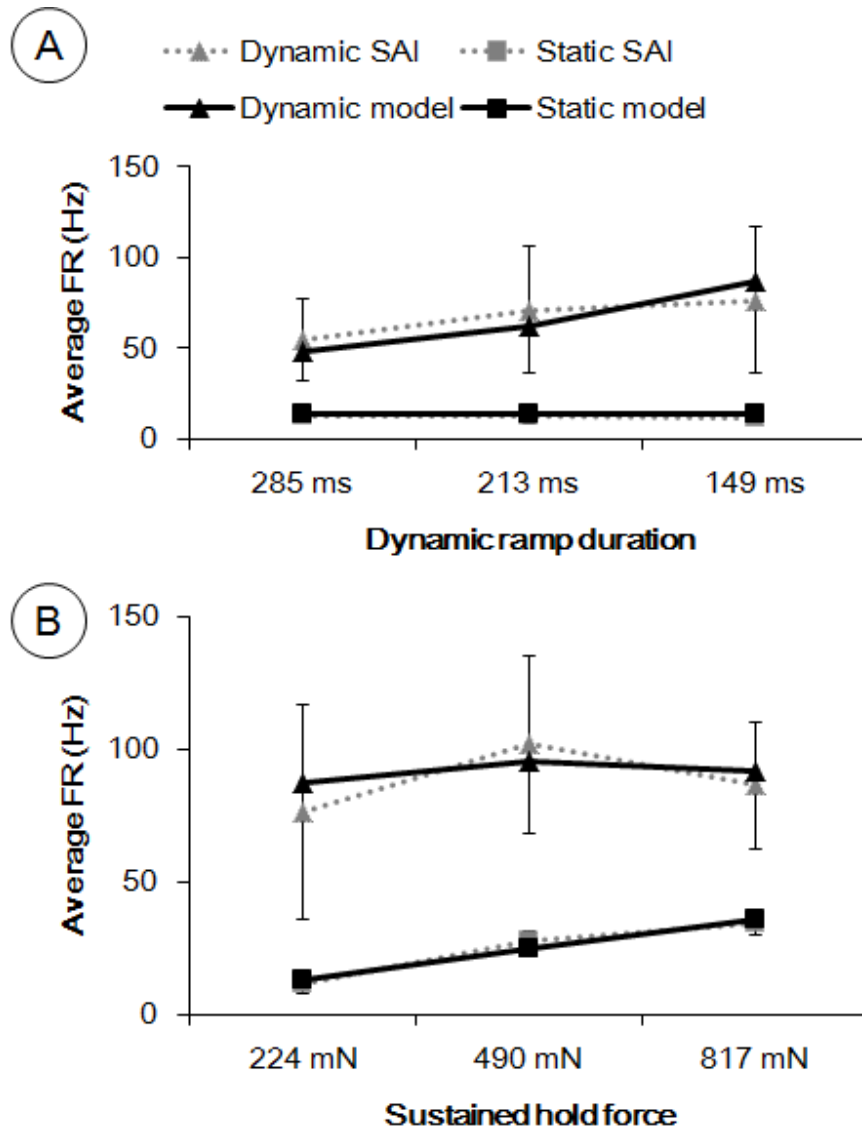


Figure 4.4. Model predictions (black) and SAI recordings (gray) showing average firing rates in dynamic ramp (square) and sustained hold (triangle) phases. A: Comparisons at different ramp times; B: Comparisons at different sustained force.

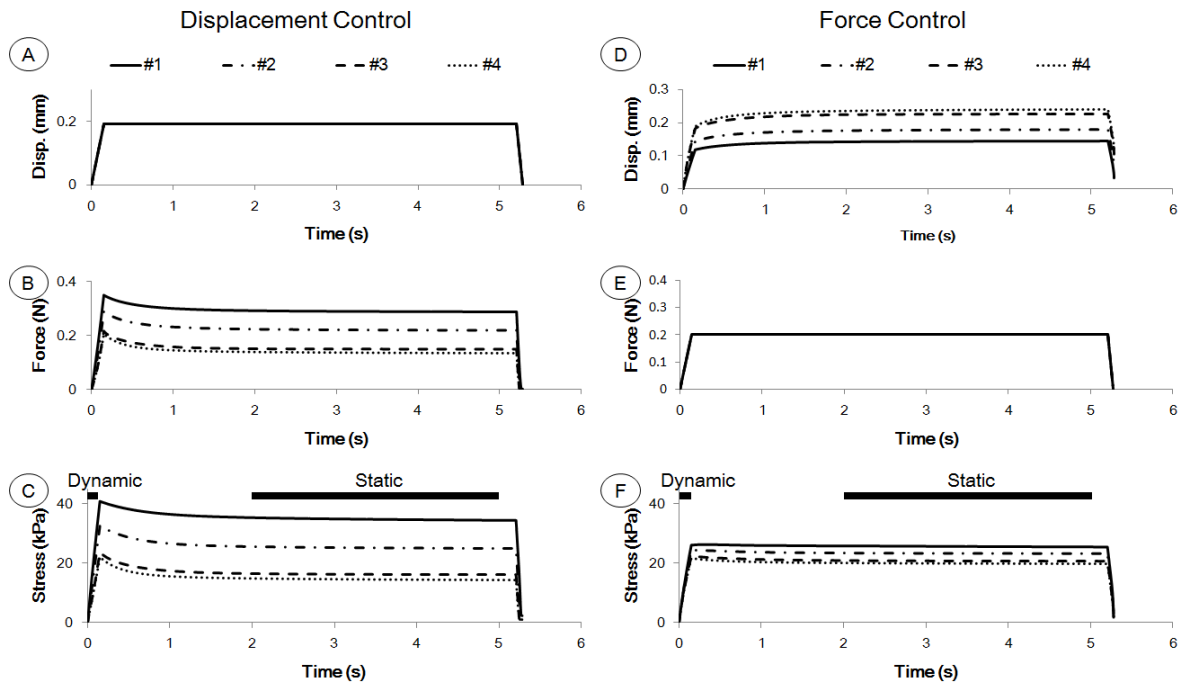


Figure 4.5 FE results using skin measurements #1-4. A-C: displacement trace, force trace and maximum compressive stress at receptor site, under displacement-controlled mechanical stimuli. D-F: displacement trace, force trace and maximum compressive stress at receptor site, under force-controlled mechanical stimuli.

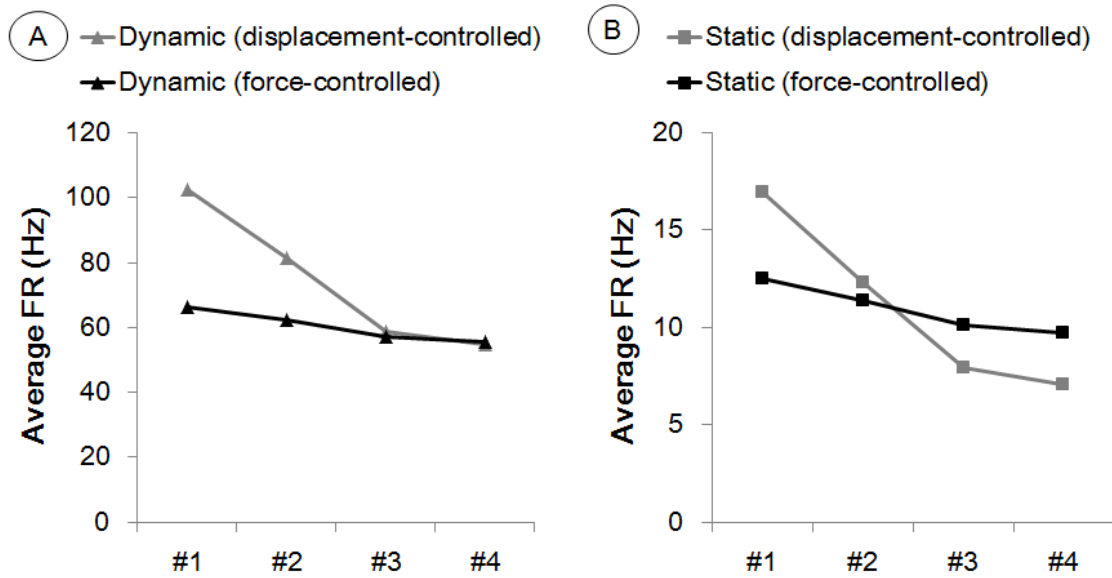


Figure 4.6 SAI simulation results of sample #1-4 under displacement-controlled stimuli (grey) and force-controlled stimuli (black). A: The variation of average firing rates at dynamic phase (triangle); B: variation of average firing rates at static phase (square). Force-controlled results are much less variable compared to displacement-controlled ones.

Exploratory numerical experiments. The outputs of FE models are shown in Figure 4.5.

The maximum compressive stress traces from models with displacement control stimuli were significantly more variant than those from models with force control stimuli. Predicted neural outputs gave similar results, as the average firing rates with different skin thicknesses was much steadier for force-controlled stimuli compared with displacement control (Figure 4.6). A quantitative comparison of standard deviations between two indentation methodologies is shown in Table 4.2, where the variance of displacement-controlled response is ~3–5 greater than that from force-controlled stimuli.

Table 4.2 Comparison of variation between displacement and force control stimuli

Stimuli control	SD of firing rate (Hz)		SD of stress (Pa)		SD of stress rate (Pa/s)	
	Dynamic ramp	Sustained hold	Dynamic	Static	Dynamic	Static
Displacement	22.17	4.55	4819.42	9337.80	59287.87	84.16
Force	4.94	1.27	909.17	2596.20	13458.48	28.06
Ratio	4.49	3.59	5.30	3.60	4.40	3.00

4.4. Discussion

Our modeling results indicate that force control may lead to less variation in neural responses between individuals. This is due to the biological observation, in the mouse, that between-animals the hyper-elasticity of the skin remains relatively consistent, though there are drastic differences in skin thickness. In specific, the variability in skin thickness much less impacts the predicted SAI response under control of the stimulus by force, by ~25%, as compared to control by displacement (Table 2). Existing tactile display devices rely upon both force [46] and displacement control [39]. One of the desired characteristics of these devices is reliability of stimulus delivery independent of end-user, and therefore the results of this work argue for employing force-controlled technologies.

The time-dependent visco-elastic parameters of the mouse skin also varies significantly between-animals, as noted in Table 1, but do not stand out as a major factor in our results, because of how we setup our dependent metrics. Our window for calculating static firing rate window is set at 2-5 seconds, as has been done by others before [49], which is well

after the point that the skin has relaxed from the beginning the of stimulus hold. The stimulus ramp, on the other hand, happens so rapidly (~ 100 ms) that the viscoelasticity is minimal relative to the contribution of the hyperelasticity. A further analysis might consider the impact of the visco-elastic decay over the time-frame of the beginning of the hold to about 1-2 seconds, and there likely might be a correlation with the firing rate [25]. Finally, note that the neural responses of SAI afferents vary significantly between animals [50], and the source of such variation may come from the biological events which constitute our touch perception: the object in the environment first contacts and deforms the skin, and these spatial distributions of forces propagate through the skin to the locations of the end organs. Local stresses/strains are transduced into trains of action potentials and then carried by somatoensory afferents to the central nervous system. For SAI afferents, at least three factors impact the transfer function: a) mechanical properties of the skin which modulate the distal stimulus to stress/strain local to Merkel cells; b) transduction properties at individual Merkel cell-neurite complexes; c) branch-structured morphology of the SAI afferent, which integrates information from Merkel cell-neurite complexes. Given the many sources of natural variation in propagation of a touch stimulus to receptors, it is essential that measures are taken to minimize experimental variables. However, only the mechanical properties of the skin were analysed herein. In the future, we will confirm our modeling result with neurophysiological recordings, from the skin of animals of known difference in thickness.

5. Overall Thesis Conclusion

Overall, work herein has mainly conclusions from three aspects, respectively on the analysis of skin's nonlinear spatial property (hyperelasticity), nonlinear temporal property (viscoelasticity) and impact of skin's nonlinearity on SAI response.

There are three major findings in this work. First of all, we know that given specific skin site, the modulus of skin material generally remains constant, while thickness and stiffness vary significantly. This is important conclusion, which gives rationale for common modeling practice of assigning a single value for skin modulus across all ages. Second, we know that the viscoelasticity is highly nonlinear: it is loading velocity dependent as well as thickness dependent. Therefore, for electrophysiological recordings it is necessary to control the stimuli at constant loading rate, as well as measure the thickness of specific skin specimens. Third, we explored the different loading methodologies, namely displacement and force controlled stimuli. Numerical simulations indicate that by use of force-controlled stimuli, the variation in neural responses would be minimized.

The work herein has two major implications. First of all, upon the design of haptic devices/interfaces, the stimuli type is preferred to be controlled by force in contrast with controlled by displacement, in order to diminish variation of perceived signal due to skin mechanical properties variation. Existing tactile display devices rely upon both force [21]

and displacement control [8]; one of the desired characteristics of these devices is reliability of stimulus delivery independent of end-user, and therefore the results of this work argue for employing force-controlled technologies. Secondly, upon the design of experiments seeking to understand the underlying principles of mechanotransduction, we would recommend the control of stimuli type via force as adopted by psychophysics researches on e.g. grating orientation [4], sphere size [5] or spatial anisotropy [6], and also the measurement of skin thickness as well as loading velocity in the future, since neural response are known to be dependent on these variables.

However, this study only focuses on single-unit level responses. To facilitate the design of new-generation haptic interfaces as well as neural prosthetics, population responses, within receptor type as well as across receptor types are necessary, which is a potential field for future work.

Appendix A: Derivations of equations for Section 2

Derivation of Eqn. (2.5)

Stiffness is defined by force over displacement. Therefore, initial stiffness k_0 can be derived by:

$$k_0 = \left. \frac{\partial F}{\partial d} \right|_{d=0} \xrightarrow{\text{Plug in Eqn.(3)}} k_0 = \left. \frac{\partial [F_T(e^{pd}-1)]}{\partial d} \right|_{d=0} = (pF_T e^{pd}) \Big|_{d=0} = pF_T, \quad (\text{A1.1})$$

Derivation of Eqn. (2.6)

Modulus is defined by stress over strain. Therefore, initial stiffness k_0 can be derived by:

$$E_0 = \left. \frac{\partial \sigma}{\partial \varepsilon} \right|_{\varepsilon=0} \xrightarrow{\text{Plug in Eqn.(4)}} E_0 = \left. \frac{\partial [\sigma_T(e^{q\Delta\lambda}-1)]}{\partial \varepsilon} \right|_{\varepsilon=0}, \quad (\text{A1.2})$$

where ε denotes strain. Note that

$$\lim_{\varepsilon \rightarrow 0} \varepsilon = \Delta\lambda, \quad (\text{A1.3})$$

Therefore, we have

$$E_0 = \left. \frac{\partial [\sigma_T(e^{q\Delta\lambda}-1)]}{\partial \varepsilon} \right|_{\varepsilon=0} = \left. \frac{\partial [\sigma_T(e^{q\Delta\lambda}-1)]}{\partial \Delta\lambda} \right|_{\Delta\lambda=0} = (q\sigma_T e^{q\Delta\lambda}) \Big|_{\Delta\lambda=0} = q\sigma_T, \quad (\text{A1.4})$$

Derivation of Eqn. (2.7)

Divide the RHS and LHS of Eqn. (2.3) by the RHS and LHS of Eqn. (2.4)

correspondingly, we have

$$\frac{F}{\sigma} = \frac{F_T(e^{pd}-1)}{\sigma_T(e^{q\Delta\lambda}-1)}, \quad (\text{A1.5})$$

Note that $\sigma_T = \frac{F_T}{A}, \sigma = \frac{F}{A}$. Therefore,

$$A = A \frac{e^{pd}-1}{e^{q\Delta\lambda}-1} \xrightarrow{\text{Cancel } A \text{ out}} e^{pd} - 1 = e^{q\Delta\lambda} - 1. \quad (\text{A1.6})$$

Organize, we get

$$p = q \frac{\Delta\lambda}{d}. \quad (\text{A1.7})$$

Plug in Eqn. (2.1-2.2), and note that $d = l_0 - l$,

$$p = \frac{1-\frac{l}{l_0}}{l_0-1} q = \frac{q}{l_0}. \quad (\text{A1.8})$$

Which is the same with Eqn (2.7).

Appendix B: Case study for Section 3 in strain-dependency on one sample

Methods

Test methods for case study on strain-dependency. The viscoelasticity of the skin was also tested, whereby the compressive strain, for one skin specimen, was varied at 10 levels. One additional animal, 9.57 weeks old with body weight of 19.63 grams, was used in this small case study. Only the NT skin site was tested under only the fast loading velocity, at the 10 levels of strain (Figure A2.1A) of equal increments. Similar to the previous procedures, data from the 6th run of 10 repetitions at each level of strain was analyzed in order to avoid variance introduced by loading history. Since the fast loading velocity was adopted, the loading phase in analyzing the strain-dependency was simplified into an ideal step load

$$\lambda(t) = \begin{cases} 1, & x < 0 \\ \lambda_{min}, & x \geq 0 \end{cases} \quad (\text{A2.1})$$

where λ_{min} denotes the stretch under full load. By inserting Eqn. (3.5) into Eqn. (3.1) and integrate the Dirac delta function, we attain

$$\sigma(t) = G(t)\sigma_e(\lambda_{min}). \quad (\text{A2.2})$$

Note that $\sigma_e(\lambda_{min})$ is equivalent to the stress at time zero σ_0 . We also substituted t_k with t , and moved $G(t)$ to the left hand side,

$$G(t) = \frac{\sigma(t)}{\sigma_0}, \quad (\text{A2.3})$$

to get the reduced relaxation function, which has the same form of Prony series Eqn. (3.3), as defined before. Among strain measures such as true strain, Biot strain and Green strain, Green strain was used, as defined in finite deformation,

$$\varepsilon = \frac{(\lambda^2 - 1)}{2}. \quad (\text{A2.4})$$

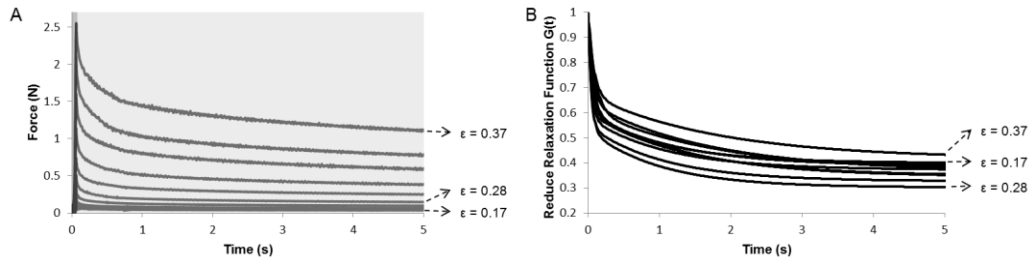


Figure A2.1 A: Force traces under ten levels of strain. The two phases (ramp and hold) are shaded uniquely. B: Fitted reduced relaxation functions under the ten levels of strain, three examples of which are denoted on the right (17%, 28% and 37% strain). Note that five pre-indentation traces are not shown.

Force-time data (Figure A2.1A) from the experiment on strain-dependency were converted to stress-time data by dividing force over sample area, smoothed via cubic spline to attain more accurate peak stress values, then normalized by the peak force of each trace (Eqn. (A2.3)) before fitting to the Prony series of Eqn. (3.3). The fitting returned an average R^2 value of 0.98, with 10 resultant reduced relaxation functions $G(t)$ as shown in Figure A2.1B.

Results

Dependency of tissue viscoelasticity on level of strain. As strain increases, before a strain

of 0.28 we observe greater relaxation at the same time constants, and after 0.28 less relaxation at longer time constants. In specific, these two strain regions were observed: region I from a strain of 0.17 to 0.28; region II from a strain of 0.28 to 0.37, Figure 5A. For example, when level of strain increases from 0.17 to 0.28 the time scale of the relaxation almost remains unchanged but $G(t)$ at 0.28 relaxes more than that of 0.17. Again, when level of strain increases from 0.28 to 0.37 the time scale is postponed while $G(t)$ relaxes less in 0.37 to 0.28. With fitted parameters we note that in region I, the two time constants (τ_1 and τ_2) remained steady (Figure A2.2C) as G_1 , G_2 increased with level of strain and G_∞ decreased with level of strain (Figure A2.2B). In region II, both time constants increased with level of strain (Figure A2.2C) while G_1 decreased, G_2 remained constant and G_∞ increased with level of strain (Figure A2.2B). Each increase and decrease passed Pearson test of correlation, as listed in Table A2.1.

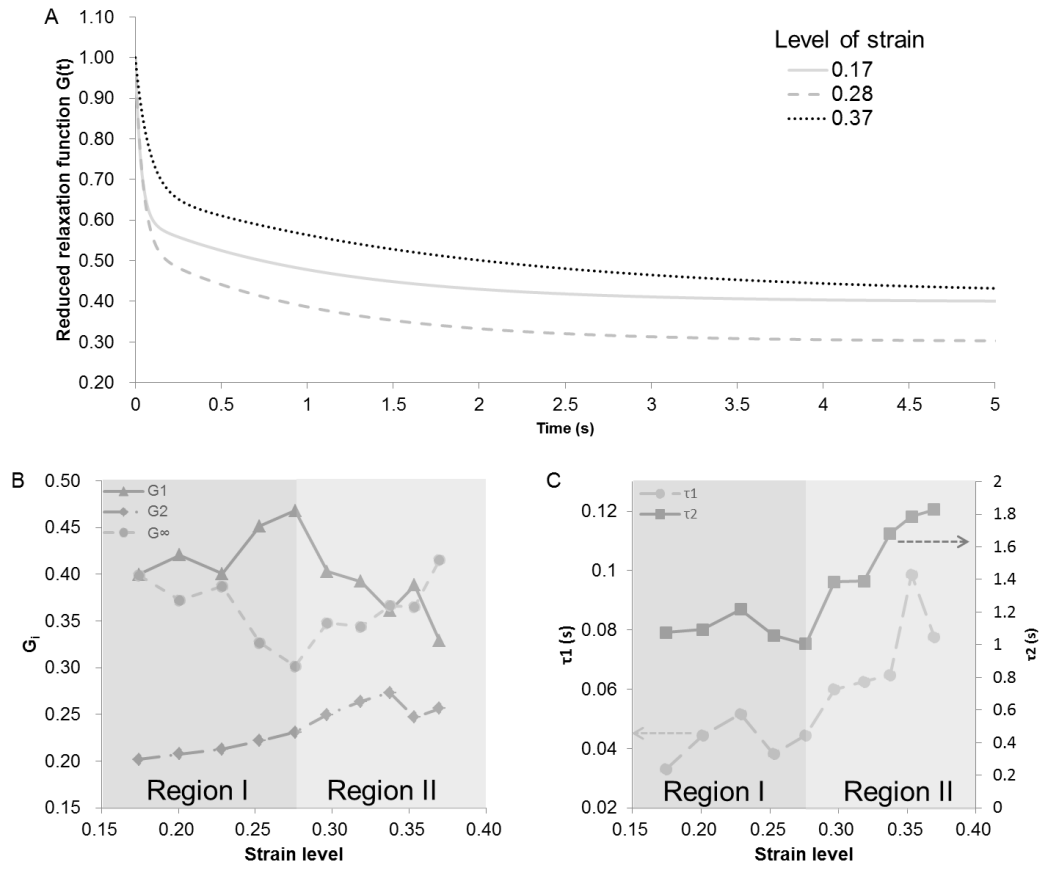


Figure A2.2 A: Three typical reduced relaxation functions. B: Values of G_i when level of strain varies. C: Values of time constants when level of strain varies.

Table A2.1 Correlation coefficients between level of strain and viscoelastic parameters τ and G_i in region I and II.

	τ_1	τ_2	G_1	G_2	G_∞
Region I	0.40***	-0.32***	0.85*	0.99	-0.90
Region II	0.83	0.96	-0.90	0.52***	0.92

*** denotes $p\text{-value} > 0.5$; ** denotes $0.1 < p\text{-value} < 0.5$; * denotes $0.05 < p\text{-value} < 0.1$; others $p\text{-value} < 0.05$. Grey-scale shading is used to denote positive/negative/neutral correlation.

Discussion

Biological reasoning for dependency on level of strain and loading rate of skin relaxation.

The viscoelasticity of skin owes itself to two characteristics of its components, the viscosity of interstitial fluid [15], and complex matrix structure of collagen and elastin solid [7]. These two characteristics can be mapped to the two-region behavior observed when varying the level of strain, that 1) when finite deformation begins (region I in Figure A2.2A and B) the interstitial fluid viscosity dominates since it is mostly free fluid movement; 2) at a later point (strain = 0.28 in this case) the matrix structure of elastin, and to some extent collagen, dominate a more typical solid elasticity (region II in Figure A2.2A and B).

Acknowledgment

This work was supported by a grant from the National Institutes of Health (NINDS R01NS073119 to EAL and GJG). The content is solely the responsibility of the authors and does not necessarily represent the official views of the National Institutes of Health. The author would like to thank Professor Ellen A. Lumpkin for providing data used in the analysis and insight regarding the analytical methods. The author would also like to thank Elmer K. Kim in help of analyzing electrophysiological data.

Reference

- [1] K. Johnson, “The roles and functions of cutaneous mechanoreceptors,” *Current Opinion in Neurobiology*, vol. 11, no. 4, pp. 455–461, Aug. 2001.
- [2] T. Maeno, K. Kobayashi, and N. Yamazaki, “Relationship between the structure of human finger tissue and the location of tactile receptors,” *lab.sdm.keio.ac.jp*.
- [3] G. J. Gerling and G. W. Thomas, “Fingerprint lines may not directly affect SA-I mechanoreceptor response,” *Somatosensory & motor research*, vol. 25, no. 1, pp. 61–76, Mar. 2008.
- [4] G. J. Gerling, “SA-I mechanoreceptor position in fingertip skin may impact sensitivity to edge stimuli,” *Applied bionics and biomechanics*, vol. 7, no. 1, pp. 19–29, Mar. 2010.
- [5] W. R. Loewenstein, “Mechano-electric transduction in the Pacinian corpuscle. Initiation of sensory impulses in mechanoreceptors,” *Handbook of Sensory Physiology. I. Principles of Receptor Physiology*, pp. 269–290.
- [6] C. H. Daly, “Biomechanical Properties of Dermis,” *Journal of Investigative Dermatology*, vol. 79, no. s1, p. 17s–20s, Jul. 1982.
- [7] J. Wu, R. Dong, W. Smutz, and A. Schopper, “Nonlinear and viscoelastic characteristics of skin under compression: experiment and analysis,” *Bio-Medical Materials and ...*, vol. 13, no. 4, pp. 373–385, 2003.
- [8] T. C. Battaglia, “GDF-5 deficiency alters stress-relaxation properties in mouse skin,” *Journal of dermatological science*, vol. 39, no. 3, pp. 192–5, Sep. 2005.
- [9] C. H. Daly and G. F. Odland, “Age-related Changes in the Mechanical Properties of Human Skin,” *Journal of Investigative Dermatology*, vol. 73, no. 1, pp. 84–87, Jul. 1979.
- [10] P. G. Agache, C. Monneur, J. L. Leveque, and J. De Rigal, “Mechanical properties and Young’s modulus of human skin in vivo,” *Archives of dermatological research*, vol. 269, no. 3, pp. 221–32, Jan. 1980.
- [11] K. Dandekar, B. I. Raju, and M. A. Srinivasan, “3-D finite-element models of human and monkey fingertips to investigate the mechanics of tactile sense,” *Journal of biomechanical engineering*, vol. 125, no. 5, pp. 682–91, Oct. 2003.

- [12] J. R. Phillips and K. O. Johnson, "Tactile spatial resolution. III. A continuum mechanics model of skin predicting mechanoreceptor responses to bars, edges, and gratings.," *Journal of neurophysiology*, vol. 46, no. 6, pp. 1204–25, Dec. 1981.
- [13] Z. Zaidi and S. Lanigan, "Skin: Structure and Function," *Dermatology in Clinical Practice*, pp. 1–15, 2010.
- [14] H. Eshel and Y. Lanir, "Effects of Strain Level and Proteoglycan Depletion on Preconditioning and Viscoelastic Responses of Rat Dorsal Skin," *Annals of Biomedical Engineering*, vol. 29, no. 2, pp. 164–172, Feb. 2001.
- [15] C. W. J. Oomens, D. H. van Campen, and H. J. Grootenboer, "A mixture approach to the mechanics of skin," *Journal of Biomechanics*, vol. 20, no. 9, pp. 877–885, Jan. 1987.
- [16] O. Lokshin and Y. Lanir, "Viscoelasticity and preconditioning of rat skin under uniaxial stretch: microstructural constitutive characterization.," *Journal of biomechanical engineering*, vol. 131, no. 3, 2009.
- [17] C. Edwards and R. Marks, "Evaluation of biomechanical properties of human skin," *Clinics in dermatology*, vol. 13, no. 4, pp. 375–380, 1995.
- [18] Y. Lanir and Y. C. Fung, "Two-dimensional mechanical properties of rabbit skin—II. Experimental results," *Journal of Biomechanics*, vol. 7, no. 2, pp. 171–182, Mar. 1974.
- [19] P. G. Martin, "Properties of human skin," University of Virginia, United States -- Virginia.
- [20] C. Escoffier, J. de Rigal, A. Rochefort, R. Vasselet, J.-L. Leveque, and P. G. Agache, "Age-Related Mechanical Properties of Human Skin: An In Vivo Study.," *Journal of Investigative Dermatology*, vol. 93, no. 3, pp. 353–357, Sep. 1989.
- [21] N. Krueger, S. Luebberding, M. Oltmer, M. Streker, and M. Kerscher, "Age-related changes in skin mechanical properties: a quantitative evaluation of 120 female subjects.," *Skin research and technology : official journal of International Society for Bioengineering and the Skin (ISBS) [and] International Society for Digital Imaging of Skin (ISDIS) [and] International Society for Skin Imaging (ISSI)*, vol. 17, no. 2, pp. 141–8, May 2011.
- [22] J. Whitton, "New values for epidermal thickness and their importance," *Health Physics*, vol. 24, no. 1, pp. 1–8, 1973.

- [23] L. Smalls, "Effect of dermal thickness, tissue composition, and body site on skin biomechanical properties," *Skin research and ...*, vol. 12, no. 1, pp. 43–49, 2006.
- [24] S. Müller-Röver, B. Handjiski, C. van der Veen, S. Eichmüller, K. Foitzik, I. A. McKay, K. S. Stenn, and R. Paus, "A comprehensive guide for the accurate classification of murine hair follicles in distinct hair cycle stages.," *The Journal of investigative dermatology*, vol. 117, no. 1, pp. 3–15, Jul. 2001.
- [25] S. A. Wellnitz, D. R. Lesniak, G. J. Gerling, and E. A. Lumpkin, "The regularity of sustained firing reveals two populations of slowly adapting touch receptors in mouse hairy skin.," *Journal of Neurophysiology*, vol. 103, no. 6, pp. 3378–3388, 2010.
- [26] B. H. Pubols, "Factors affecting cutaneous mechanoreceptor response. I. Constant-force versus constant-displacement stimulation.," *Journal of neurophysiology*, vol. 47, no. 3, pp. 515–29, Mar. 1982.
- [27] M. A. Serrat, C. J. Vinyard, and D. King, "Alterations in the mechanical properties and composition of skin in human growth hormone transgenic mice.," *Connective tissue research*, vol. 48, no. 1, pp. 19–26, Jan. 2007.
- [28] G. Holzapfel, "Nonlinear Solid Mechanics: A Continuum Approach for Engineering," 2000.
- [29] Y. Wang, K. L. Marshall, Y. Baba, G. J. Gerling, and E. A. Lumpkin, "Compressive measurement of mouse skin indicates systematic trends in thickness and stiffness with age and body weight and constant but variable modulus," *Journal of Investigative Dermatology*.
- [30] Y. Fung and S. Cowin, "Biomechanics: Mechanical properties of living tissues," *Journal of Applied Mechanics*, 1994.
- [31] E. K. Kim, G. J. Gerling, S. M. Bourdon, S. A. Wellnitz, and E. A. Lumpkin, "Force sensor in simulated skin and neural model mimic tactile sai afferent spiking response to ramp and hold stimuli," *Journal of NeuroEngineering and Rehabilitation*, vol. 9, no. 1, p. 45, 2012.
- [32] A. L. Williams, G. J. Gerling, S. A. Wellnitz, S. M. Bourdon, and E. A. Lumpkin, "Skin relaxation predicts neural firing rate adaptation in SAI touch receptors.," in *Conference proceedings : Annual International Conference of the IEEE Engineering in Medicine and Biology Society. IEEE Engineering in Medicine and Biology Society. Conference*, 2010, vol. 2010, pp. 6678–81.

- [33] S. M. Maricich, S. A. Wellnitz, A. M. Nelson, D. R. Lesniak, G. J. Gerling, E. A. Lumpkin, and H. Y. Zoghbi, "Merkel cells are essential for light-touch responses.," *Science (New York, N.Y.)*, vol. 324, no. 5934, pp. 1580–2, Jun. 2009.
- [34] K. O. Johnson, "Neural Coding," *Neuron*, vol. 26, no. 3, pp. 563–566, Jun. 2000.
- [35] J. C. Craig, "Grating orientation as a measure of tactile spatial acuity," *Somatosensory & Motor Research*, vol. 16, no. 3, pp. 197–206, Jan. 1999.
- [36] A. W. Goodwin, K. T. John, and A. H. Marceglia, "Tactile discrimination of curvature by humans using only cutaneous information from the fingerpads," *Experimental Brain Research*, vol. 86, no. 3, Sep. 1991.
- [37] G. O. Gibson and J. C. Craig, "Tactile spatial sensitivity and anisotropy," *Perception & Psychophysics*, vol. 67, no. 6, pp. 1061–1079, Aug. 2005.
- [38] G. Westling and R. S. Johansson, "Factors influencing the force control during precision grip," *Experimental Brain Research*, vol. 53, no. 2, Jan. 1984.
- [39] A. P. Sripati, S. J. Bensmaia, and K. O. Johnson, "A continuum mechanical model of mechanoreceptive afferent responses to indented spatial patterns.," *Journal of neurophysiology*, vol. 95, no. 6, pp. 3852–64, Jun. 2006.
- [40] T. Maeno, K. Kobayashi, and N. Yamazaki, "Relationship between the Structure of Human Finger Tissue and the Location of Tactile Receptors.," *JSME International Journal Series C*, vol. 41, no. 1, pp. 94–100, 1998.
- [41] M. A. Srinivasan, "Surface deflection of primate fingertip under line load.," *Journal of biomechanics*, vol. 22, no. 4, pp. 343–9, Jan. 1989.
- [42] J. R. Phillips and K. O. Johnson, "Tactile spatial resolution. II. Neural representation of Bars, edges, and gratings in monkey primary afferents.," *Journal of neurophysiology*, vol. 46, no. 6, pp. 1192–203, Dec. 1981.
- [43] P. S. Khalsa, R. M. Friedman, M. A. Srinivasan, and R. H. Lamotte, "Encoding of shape and orientation of objects indented into the monkey fingerpad by populations of slowly and rapidly adapting mechanoreceptors.," *Journal of neurophysiology*, vol. 79, no. 6, pp. 3238–51, Jun. 1998.
- [44] I. Birznieks, P. Jenmalm, A. W. Goodwin, and R. S. Johansson, "Encoding of direction of fingertip forces by human tactile afferents.," *The Journal of*

neuroscience : the official journal of the Society for Neuroscience, vol. 21, no. 20, pp. 8222–37, Oct. 2001.

- [45] K. I. Baumann, W. Hamann, and M. S. Leung, “Mechanical properties of skin and responsiveness of slowly adapting type I mechanoreceptors in rats at different ages.,” *The Journal of physiology*, vol. 371, pp. 329–37, Feb. 1986.
- [46] S. A. Wall and S. Brewster, “Sensory substitution using tactile pin arrays: Human factors, technology and applications,” *Signal Processing*, vol. 86, no. 12, pp. 3674–3695, Dec. 2006.
- [47] Y. C. Fung and S. C. Cowin, “Biomechanics: Mechanical Properties of Living Tissues, 2nd ed.,” *Journal of Applied Mechanics*, vol. 61, no. 4, p. 1007, 1994.
- [48] P. S. Khalsa, R. H. Lamotte, and P. Grigg, “Tensile and Compressive Responses of Nociceptors in Rat Hairy Skin,” *J Neurophysiol*, vol. 78, no. 1, pp. 492–505, Jul. 1997.
- [49] A. Iggo and A. R. Muir, “The structure and function of a slowly adapting touch corpuscle in hairy skin.,” *The Journal of physiology*, vol. 200, no. 3, pp. 763–96, Feb. 1969.
- [50] D. R. Lesniak, S. A. Wellnitz, G. J. Gerling, and E. A. Lumpkin, “Statistical analysis and modeling of variance in the SA-I mechanoreceptor response to sustained indentation.,” *Conference proceedings : Annual International Conference of the IEEE Engineering in Medicine and Biology Society. IEEE Engineering in Medicine and Biology Society. Conference*, vol. 2009, pp. 6814–7, Jan. 2009.